# Chapter 6
# Phase Control of $TiO_2$ Photocatalyst


## 6.1 Introduction

In recent years, the environmental pollution and energy exhaustion problems are attracting more and more attention of mankind on a global scale. Due to the increase of population and industrial growth, the energy consumption has been accelerating, and a large amount of toxic agents and industrial wastes have been released into the air and waterways, leading to energy crisis, global warming, and pollution-related diseases. Thus, nowadays most scientists face the major challenges to develop the environmentally harmonious, ecologically clean, safe, and sustainable chemical technologies, materials, and processes for addressing energy as well as pollution and climatic change.

Although many different kinds of approaches to solve these issues exist, ever since Honda and Fujishima [1] found that $TiO_2$ photoelectrode could induce cleavage of water into $H_2$ and $O_2$ under the irradiation of ultraviolet light, there has been enormous increasing interest in the use of $TiO_2$ as well as other extended oxide and chalcogenide semiconductors. The organic toxic materials at low concentrations are photocatalytically converted to harmless oxidation products such as $CO_2$ and $H_2O$, achieving the purpose of the environmental remediation [2–29]. $TiO_2$ photocatalyst with a convenient bandgap of 3.2 eV (ca. 400 nm) has many attractive features including high stability, low cost, nontoxicity, good biocompatibility, and good photocatalytic performance in the oxidation of organic pollutants to $CO_2$ and $H_2O$. For these reasons, $TiO_2$-based photocatalysts have drawn much attention for various applications in the fields of energy regeneration and environmental protection.

As mentioned above, due to its excellent properties, lots of systematic in-depth studies of $TiO_2$ has been performed by the majority of scientists, promoting the application process in various aspects related to energy and environment in recent years. The related research mainly includes studies on photocatalytic mechanism [3–5], regulation of crystal structure and morphology [6–15], improvement of



J. Zhang et al., *Photocatalysis*, Lecture Notes in Chemistry 100,
https://doi.org/10.1007/978-981-13-2113-9_6

photocatalysis and photoelectric conversion efficiency [16–24], and expansion of the optical response range [25–29]. However, traditional single-phase $TiO_2$ has defects in the photocatalytic performance, which are mainly on account of two aspects: on one hand, owing to the limits of its bandgap, the absorption of visible light is little, causing the inefficient utilization of the sunlight [3–5]; on the other hand, the high recombination rate of photo-generated electrons and holes greatly limits the photocatalytic performance of $TiO_2$ [30, 31].

Researches have reported that modification of $TiO_2$ by organic dye photosensitization [32–36], noble metal deposition [37–41], or doping [42–45] or semiconductor compounding [45–49] can effectively enhance the photon utilization and reduce the recombination rate of photo-generated electrons with holes, thereby improving the photocatalytic efficiency of $TiO_2$. However, those methods have many disadvantages such as low economic effect, poor reaction stability and controllability, and complicated operation process, among others. In these respects, mixed-phase $TiO_2$ with relatively simple preparation process, low cost, and adjustable crystal type has attracted much attention. In the mixed-phase photocatalyst, the effective separation of the photo-generated electrons and holes, taken place on the two-phase interface, results in the reduction of their recombination rate. Moreover, adding rutile $TiO_2$ with a narrower bandgap into pure anatase $TiO_2$ to form mixed-phase $TiO_2$ of rutile and anatase can enhance the utilization of visible light to some extent, further significantly improving the photocatalytic activity of $TiO_2$ [50–53]. These abovementioned advantages of the mixed phase can efficiently enhance the comprehensive properties of $TiO_2$ photocatalyst. Apart from these researches, other kinds of mixed-phase $TiO_2$ have also been studied in depth, such as anatase/brookite [54, 55], anatase/brookite/rutile [56], and brookite/$TiO_2$(B) [57]. The results of these photocatalytic studies have demonstrated that the photocatalytic activity of mixed-phase $TiO_2$ is higher than that of single-phase $TiO_2$, which results from the existence of different band positions and the promoted separation rate of photo-generated electron–hole pairs and catalytic "hot spots" at the interface of different phases [51, 56].

In this chapter, first, we briefly introduce three main kinds of $TiO_2$ phases (anatase, rutile, and brookite), and then we focus on recent advances in the development of mixed-phase $TiO_2$ photocatalysts, including the synthesis for the mixed-phase catalysts and their applications to various photocatalytic reaction systems such as photocatalytic hydrogen production, photoreduction of $CO_2$, and photocatalytic degradation of organic pollutants. Following this we discuss the mechanism of enhanced photocatalytic activity of the mixed-phase $TiO_2$. Finally, the existing problems of the mixed-phase $TiO_2$ are summarized, and the application prospects of this kind of nanomaterials are outlooked.

## 6.2 Phases of $TiO_2$

$TiO_2$ possesses eight types of crystal phases, which are rutile, anatase, brookite, $TiO_2$-B, $TiO_2$-R, $TiO_2$-H, $TiO_2$-II, and $TiO_2$-III [58]. Among them, rutile, anatase, and brookite have been researched mostly for applications because they are naturally occurring oxides of titanium at atmospheric pressure [59, 60]. The other five phases have also been investigated [61–64]; however, because they are usually formed at high pressure, there is minor significance for practical research and applications. Therefore, in this chapter, we mainly focus on the three phases of rutile, anatase, and brookite.

### *6.2.1 Structure Properties of Rutile, Anatase, and Brookite*

The three kinds of $TiO_2$ phases possess different crystallographic properties, as shown in Table 6.1 [65].

In their structures, $TiO_6$ octahedron exists in a more or less tortuous configuration formed by the fundamental building block made up of a titanium atom surrounded by six oxygen atoms. In the structures of the three kinds of $TiO_2$ phase, the stacking of the $TiO_6$ octahedra causes threefold coordinated oxygen atoms. As shown in Fig. 6.1, the structural units in these three $TiO_2$ crystals form from $TiO_6$ octahedron basic units and exist in different lattice configurations. In rutile, the chains were formed by $TiO_6$ octahedra connected by sharing an edge with the c-axis and then

**Table 6.1** Crystallographic properties of anatase, rutile, and brookite $TiO_2$

| Crystal structure | Density (g/cm [3]) | System | Space group | Cell parameters (nm) | | |
|---|---|---|---|---|---|---|
| | | | | a | b | c |
| Rutile | 4.240 | Tetragonal | $D_{4b}$[14]-$P4_2/mnm$ | 0.4584 | – | 0.2953 |
| Anatase | 3.830 | Tetragonal | $D_{4a}$[19]-$I4_1/amd$ | 0.3758 | – | 0.9514 |
| Brookite | 4.170 | Rhombohedral | $D_{2h}$[15]-Pbca | 0.9166 | 0.5436 | 0.5135 |

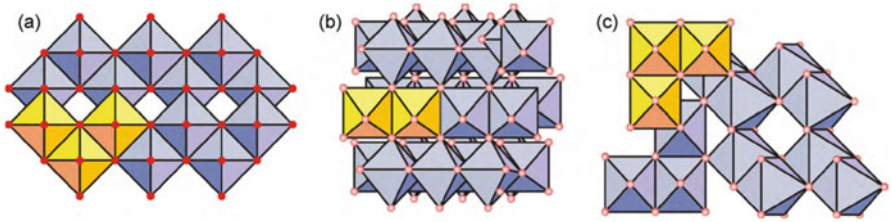


**Fig. 6.1** Crystalline structure of (**a**) anatase, (**b**) brookite, and (**c**) rutile [68]. (Reprinted with permission from Ref. [68]. Copyright 2010, Elsevier)

interlinked by sharing corner oxygen atoms to form a three-dimensional lattice. Contrarily in anatase, the three-dimensional lattice is formed only through sharing edge bonding among $TiO_6$ octahedra. It means that the octahedra in anatase share four edges and are arranged in zigzag chains while the octahedra in brookite share both edges and corners and form an orthorhombic structure [66, 67].

Researchers usually use the X-ray diffraction (XRD) experimental method to determine these crystal structures and estimate the crystal grain size of anatase, rutile, and brookite. Anatase peaks in X-ray diffraction are found at $\theta = 12.65°$, 18.9°, and 24.054°; the rutile peaks occur at $\theta = 13.75°$, 18.1°, and 27.2°, while brookite peaks emerge at $\theta = 12.65°$, 12.85°, 15.4°, and 18.1° (θ represents the X-ray diffraction angle) [69, 70].

### 6.2.2 *Stability and Phase Transformation*

Compared to the other two types of phases, rutile is the most stable phase. It is almost impossible for rutile to decompose or undergo a phase transformation even at very high temperatures. However, metastable anatase and brookite can be transformed into thermodynamically stable rutile when they are calcined to a certain temperature. There has been extensive research on the phase transfer mechanism of $TiO_2$ during the calcination process. Shannon [71] proposed that the transformation of anatase to rutile from crystallography includes a nucleation and growth process. At first, rutile nucleates on the surface of anatase and then expands to the bulk. Due to the great diversities between anatase and rutile, the transformation involving the breaking and reforming of bond processes can be reconstructed [72]. During the course of anatase transforming to rutile, the {112} planes in anatase are persisted as the {100} planes in the newly generated rutile. And Ti and O atoms synergistically rearrange in these planes by moving Ti atoms to a new location to form rutile via the breaking of two Ti–O bonds in the $TiO_6$ octahedron. As a result, the newly formed oxygen vacancies accelerate the transformation; meanwhile, Ti interstitials inhibit the phase transformation. The transformation from anatase to rutile is a nonequilibrium phase transition, which usually occurs at a certain range of temperature (400~1000 °C). During the transformation process, the calcination temperature has a great influence on the impurities, particle size, and surface area of products. Because impurities and processing atmosphere can result in different defect structure, they also strongly influence the temperature and rate of phase transition. Generally, impurities such as the oxides of Li, K, Na, Fe, Ce, and Mn usually promote the phase transformation via increasing the oxygen vacancies; on the contrary, impurities like S, P, and W usually restrain the phase transformation. A reductive atmosphere such as $H_2$ and $Cl_2$ can accelerate the transformation, while a conducive atmosphere can inhibit the phase transformation via the formation of Ti interstitials.

Artificial synthesis conduces to the preparation of anatase nanoparticles, especially the synthesis of $TiO_2$ in aqueous solution [73] for the reason that the energy of the three kinds of $TiO_2$ phases is quite close. On condition that the nanoparticles are

small enough (<13 nm), the small surface free energy will play a decisive role in the phase transformation [74]. For $TiO_2$ nanocrystals with the size smaller than 11 nm, anatase is the most stable phase, and the rutile phase with nanocrystals size bigger than 35 nm performs the thermodynamic stability. As for brookite phase, its stability lies between the anatase and rutile. In fact, as a metastable phase, the major physical parameters of brookite are between those of anatase and rutile. For example, the bandwidths of anatase and rutile are 3.19 and 3.0 eV, respectively, while that of brookite is 3.11 [75].

### *6.2.3 Photocatalytic Activity of Rutile, Anatase, and Brookite*

Among the three types of phases, anatase exhibits the highest photocatalytic activity, which is on account of the following aspects:

1. The bandgap of anatase is 3.19 eV, while that of rutile and brookite are 3.0 eV and 3.11 eV, respectively [62]. Therefore, the electron–hole pair of anatase has more positive or more negative potential, improving the oxidation ability [76].
2. The surface of anatase has a stronger adsorption ability for $H_2O$, $O_2$, and OH, which conduces to high photocatalytic activity because the adsorption capacity of the surface has a dramatic influence on the photocatalytic activity during the photocatalytic reaction, and strong adsorption capacity benefits to high activity.
3. Compared to rutile and brookite, anatase usually exhibits smaller grain size and larger specific surface area in the crystallization process, enhancing the photocatalytic activity.

However, due to the crystallization process greatly influencing the photocatalytic activity, the above rules do not suit for all situations. When the amorphous $TiO_2$ crystallize, rutile usually forms large grains with poor surface properties and thus exhibits low photocatalytic activity. Under the same conditions, if the rutile can have the same grain size and adsorption ability as anatase, it can also exhibit high photocatalytic activity. For example, Lee et al. [77] found that through the treatment of laser exposure, anatase phase of $TiO_2$ can transfer to rutile phase without the change of the specific surface area and grain size. This resultant rutile $TiO_2$ exhibited considerable high photocatalytic activity. Tsai et al. [78] fabricated anatase and rutile $TiO_2$ via different methods and investigated their photocatalytic activity for the degradation of phenol. It is found that the preparation methods as well as the calcination temperature have a remarkable influence on the photocatalytic activity of $TiO_2$ catalyzers. Under certain conditions, rutile $TiO_2$ exhibited very high catalytic activity. Therefore, whether anatase or rutile, the photocatalytic activity of materials greatly depends on the grain size and the surface properties. Apart from that, Ohno et al. [79] demonstrated that the photocatalytic activity of different phase $TiO_2$ relates to the electron acceptors in the system. When the electron acceptor is $O_2$, the photocatalytic activity of anatase is relatively higher than that of rutile. And when $Fe^{3+}$ is the electron acceptor, rutile exhibits higher catalytic activity than

anatase. This is because when $O_2$ acts as an electron acceptor, it is quite sensitive to properties of the catalyst materials in the process of the photocatalytic reactions. The surface structure and the low-energy band of rutile may make it show low transfer efficiency of electrons to $O_2$, and thus rutile exhibits low catalytic activity when $O_2$ is used as the electron acceptor. Therefore, rutile usually exhibits low photocatalytic activity based on the fact that most researchers use $O_2$ for the studies of photocatalytic reactions.

Because there have been few studies and experiments on brookite and the general products are mixed-phase $TiO_2$, including anatase/brookite [80], brookite/rutile [81], or anatase/brookite/rutile instead of pure brookite, the photocatalytic activity of brookite $TiO_2$ is quite controversial [44].

Recently, lots of studies have demonstrated that the mixed-phase $TiO_2$ crystals in an appropriate composition ratio exhibit higher photocatalytic activity than that of single-phase $TiO_2$ crystals. Bacsa et al. [82] found that the single-phase $TiO_2$ such as pure anatase or pure rutile has relatively lower photocatalytic activity, but a mixture of anatase and rutile in various ratios achieved enhanced photocatalytic activity than 100% anatase or 100% rutile, when the mixed phase in the ratio of 30% rutile and 70% anatase had the best photocatalytic activity. Thus the $TiO_2$ catalyzer with two kinds of phases has a certain synergistic effect for improving photocatalytic activities. And the commercial photocatalyst P25 with considerable high photocatalytic activity is also a kind of mixed-phase $TiO_2$ instead of single-phase $TiO_2$. Therefore, great efforts have been made to study in depth on the synthesis and photocatalysis applications of mixed-phase $TiO_2$.

## 6.3 Synthesis of Mixed-Phase $TiO_2$ Photocatalysts

It has been found that adjusting the experimental parameters of the synthesis can change the structure and properties of the three types of crystals, making the preparation of different mixed-phase $TiO_2$ come true. At present, there is a large number of methods to fabricate mixed-phase $TiO_2$, such as pulsed laser deposition (PLD), hydrothermal method, hydrolysis method, solvothermal method, microemulsion-mediated solvothermal method, solvent mixing and calcination method (SMC method), high-temperature calcination method, high-temperature vapor decomposition method, and so on [83]. In the synthesis process of mixed-phase $TiO_2$, with different preparation methods, the same factor has different effects on the mixed-phase crystals. In all kinds of synthesis methods, the mixed-phase ratio, morphology, and surface properties of photocatalysts are controllable via optimizing the experimental conditions, such as calcination temperature, pressure, concentration, and types of reagents. The ratio of different crystals in an excellent mixed-phase photocatalyst should have the ability to be tuned according to the actual demands, and the product should possess controllable shape as well as uniform dispersion and should be difficult to agglomerate. The preparation conditions and

influence parameters of mixed-phase $TiO_2$ will be discussed in the following subsection, combining concrete synthesis methods.

### 6.3.1 Hydrothermal Method and Solvothermal Method

The hydrothermal method is used most widely in the laboratory fabrication of $TiO_2$ nanomaterials [25, 84–90]. Using aqueous solution as the reaction system, through heating or other means, the target photocatalysts are often synthesized in a sealed reaction vessel (such as an autoclave), which creates an environment of high temperature and high pressure during the hydrothermal process. In this condition, with the increase of the water vapor pressure, the density and surface tension of the materials decrease, and the ion product increases, leading to the dissolution and the recrystallization of the substances which can be dissolved in water at room temperature. The hydrothermal method is one of the liquid-phase chemical synthesis methods, and its main factors influencing the properties of the product are vessel volume, reaction temperature, heating rate, and reaction time.

Chen and Sum et al. [91] fabricated highly crystalline single-phase $TiO_2$ brookite and two-phase anatase/brookite $TiO_2$ nanostructures in NaOH solutions via a simple hydrothermal method, using $TiS_2$ as the precursors. They successfully controlled the phase composition via varying the solution concentration as well as reaction time. In the reaction system, the precursors $TiS_2$ underwent a hydrolysis reaction as shown in the following two equations:

$$TiS_2 + 4\ NaOH \rightarrow Ti^{4+} + 4\ OH^- + 2\ Na_2S \tag{6.1}$$

$$Ti^{4+} + x(OH)^- \rightarrow Ti(OH)_x^{4-x} \tag{6.2}$$

The reaction began with the hydrolysis of $TiS_2$, forming $Ti^{4+}$ ion (Eq. 6.1). Then $Ti^{4+}$ reacted with $OH^-$ in the solution during the hydrothermal process (Eq. 6.2). The formation of different crystal phases is related to concentration of $OH^-$. When the concentration of $OH^-$ is low and thus the hydrolysis rate of $Ti^{4+}$ is slow, the hydrothermal reactions are more likely to form anatase $TiO_2$ via connecting $Ti^{4+}$ with $OH^-$; when the $OH^-$ concentration is high, the fast hydrolysis rate of $Ti^{4+}$ leads to the formation of mixed-phase $TiO_2$ nanomaterials of brookite and anatase. The mass fraction of brookite (B) and anatase (A) can be calculated by the following two formulas [92]:

$$W_B = K_B I_B / (K_A I_A + K_B I_B) \tag{6.3}$$

$$W_A = K_A I_A / (K_A I_A + K_B I_B) \tag{6.4}$$

In the formula, $K_A = 0.886$, $K_B = 2.721$, and $I_A$ represent the integral intensity of the strongest diffraction peaks in anatase, and $I_B$ represents that in brookite. The

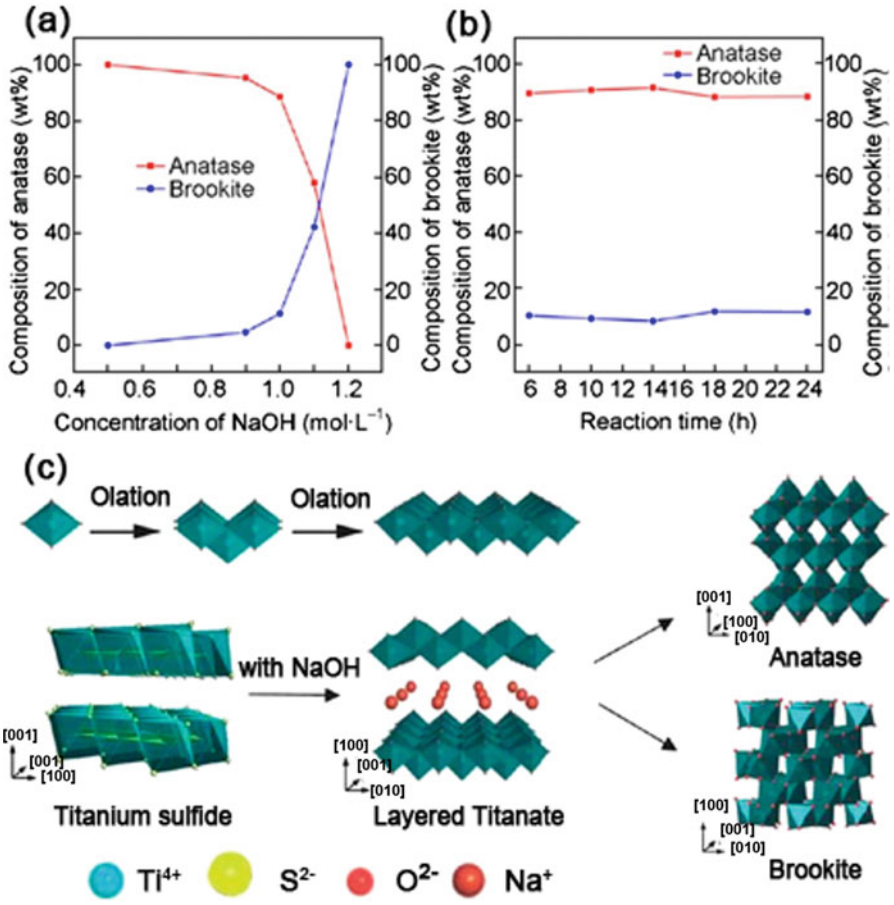


**Fig. 6.2** The composition of anatase and brookite in the mixed-phase $TiO_2$ prepared with (**a**) various NaOH concentrations and (**b**) different reaction times under hydrothermal reaction [91]; (**c**) The scheme of formation of anatase and brookite in mixed-phase $TiO_2$ [91]. (Reprinted with permission from Ref. [91]. Copyright 2013, American Chemical Society)

influences of different NaOH concentrations and distinct reaction times on $TiO_2$ crystals are shown in Fig. 6.2a, b. As NaOH concentration increases, the content of brookite increases, and when the reaction time is over 6 h, the crystalline formation of the product does not change significantly. In addition, single-phase brookite $TiO_2$ can be obtained by replacing $TiS_2$ with sodium titanate. Since $Na^+$ can stabilize the layered structure, when there is no $Na^+$ ion in the reaction system, a layered structure is instable, and the hydrothermal process causes the destruction of the structure, forming anatase $TiO_2$; when $Na^+$ is excessive, the stable layered structure does not easily collapse and ultimately form titanate; when $Na^+$ concentration is proper, the layered structure partially collapses, and part of the layered structure remains

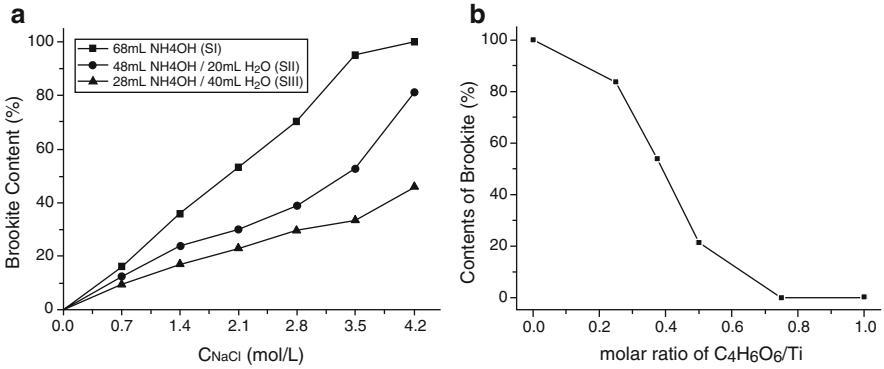


**Fig. 6.3** (**a**) Relationship between the contents of brookite and the applied NaCl concentration [93]; Reprinted with permission from Ref. [93]. Copyright 2013, Elsevier. (**b**) Relationship between the contents of brookite in the products and the applied tartaric acid to $TiCl_3$ molar ratio [97]. Reprinted with permission from Ref. [97]. Copyright 2012, Springer

instable, leading to form brookite (Fig. 6.2c). The above results are consistent with the previous literature [87].

Zhang et al. [93] simultaneously introduced NaCl and $NH_4OH$ into the hydrothermal reaction system with $TiCl_3$ as a titanium source. The results showed that changing the concentration of NaCl and the volume ratio of $NH_4OH$ to $H_2O$ can well control the phase composition of the products in the reaction system (Fig. 6.3a). They put forward that $Na^+$ was able to stabilize the layered structure of titanate, which was formed by the hydrolysis reaction of $TiCl_3$ in aqueous ammonia in the hydrothermal system. In the absence of NaCl, $NH^{4+}$ ions which exist in the interlayer of titanate can balance the negative charges of the layered titanate. However, during the process of hydrothermal treatment with high temperature up to 200 °C, $NH^{4+}$ is hydrolyzed to form $NH_4OH$ and thus is released from the interlayer. Then the $H^+$ ions generated from the hydrolysis of $NH^{4+}$ ions induce a hydroxyl condensation reaction, forming anatase $TiO_2$. In the presence of NaCl, $Na^+$ ions benefit to stabilize the layered structure with $NH_4^+$. The simultaneous existence of $Na^+$ and $NH_4^+$ in the interlayer of titanate helps to balance the negative charges of titanate. After the layered titanate was continuously treated by hydrothermal methods at a high temperature for several hours, the increased hydrolysis of $NH_4^+$ caused the collapse of layered structures. However, some bonds in the structure were kept by $Na^+$ ions. Hence the structural transformation was delayed which resulted in forming a brookite-like structure [94–96]. A brookite lattice was formed by the expansion of as-formed brookite-like structure. Increasing the concentration of NaCl would be helpful for the brookite lattice to compete with the anatase lattice. Therefore, with the increase of NaCl concentration, the brookite content in the mixed-phase $TiO_2$ increased. In addition to this research, Zhang et al. [97] developed another facial hydrothermal method for the synthesis of anatase/brookite $TiO_2$ using tartaric acid ($C_4H_6O_6$) as the phase content regulator, $TiCl_3$ as the titanium source, and NaOH to adjust the pH of the reaction solution. Changing the molar ratio of $C_4H_6O_6$ to $TiCl_3$

in the hydrothermal reaction system could successfully control the contents of brookite and anatase in the $TiO_2$ particles (Fig. 6.3b). According to the ligand field theory, they explained the mechanism of the phase evolution between brookite and anatase in which $C_4H_6O_6$ could chelate with Ti to form a stable titanium complex [98]. When the $C_4H_6O_6/TiCl_3$ molar ratio was below 0.75 in the reaction system, there were two forms of Ti species. They were the insoluble Ti-contained species Ti $(OH)_4$ and the soluble Ti-contained complex [Ti(OH)x($C_4H_6O_6$)y]z-. Under hydrothermal treatment, the amorphous $Ti(OH)_4$ could first transform to layered titanate. Given a proper concentration of $Na^+$ and $OH^-$, the layered titanate would be transformed to brookite [94]. Due to the large steric hindrance of carboxylic acidic ligands, the [Ti(OH)x($C_4H_6O_6$)y]z- complexes were inclined to combine together by sharing equatorial or apical edges and being arranged in zigzag chains, which was beneficial to form anatase crystallites, thus resulting in an mixed-phase $TiO_2$ of anatase and brookite. They also pointed out that the brookite as the pure phase or the main phase could not be obtained on the conditions that the pH value of the reaction system was lower than 9 or the hydrothermal temperature was below 180 °C. In other words, it was hard to control the contents of anatase and brookite in samples just by changing the $C_4H_6O_6/TiCl_3$ molar ratio while pH < 9 or temperature < 180 °C in the hydrothermal reaction system.

A variation of the hydrothermal method is the solvothermal method wherein many kinds of organic solvents such as ethanol, glycol, and toluene can be used to replace an aqueous system. Similar to the hydrothermal method, both the crystal types and morphology of the $TiO_2$ nanomaterials can be well controlled by regulating parameters in the solvothermal reaction system, including temperature and pressure inside the system, the reaction time, and the titanium source.

Through the solvothermal method, Li et al. [99] synthesized anatase/rutile mixed-phase $TiO_2$ crystals with different rutile content by hydrolysis of tetraisopropyltitanate in an acid alcoholic solution and studied influence of hydrochloric acid on the rutile content in the mixed-phase crystal. The results showed that high $H_2O$/Ti mole ratio favored the formation of brookite/anatase mixed-phase $TiO_2$, and low $H_2O$/Ti mole ratio benefited to form anatase/rutile mixed-phase $TiO_2$. Lei et al. [100] prepared anatase/rutile mixed-phase $TiO_2$ crystal using a low-temperature (80 °C) solvothermal method by pre-oxidizing $TiCl_3$ into $Ti^{4+}$ with $HNO_3$ followed by diluting with urea, water, and ethanol. They found that the anatase content in the mixed-phase crystal increased by increasing ethanol content in the solution (Fig. 6.4). The average particle size of anatase and rutile in the mixed-phase crystal is both below 10 nm calculated by the Scherrer formula.

The mixed-phase $TiO_2$ nanomaterials synthesized by hydrothermal and solvothermal methods are usually well crystallized and are not required to be calcinated at a certain high temperature. The size and phase type of $TiO_2$ can be regulated by simply adjusting the experimental parameters such as the type of base or acid in the reaction system, the reaction temperature, the heating rate, the reaction time, and the autoclave pressure. Besides these advantages, there still remain some drawbacks such as the requirement for the equipment to withstand high pressure as well as high temperature and experimental safety concerns. Moreover, it is difficult

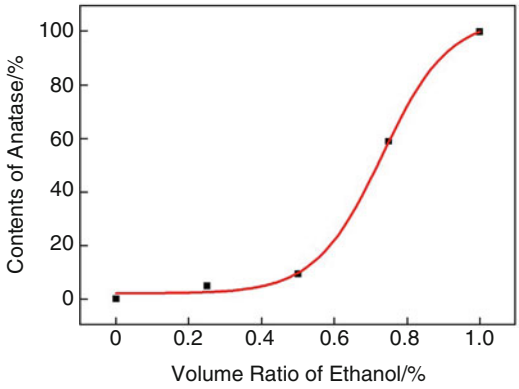


**Fig. 6.4** Relationship between the contents of anatase in the product and the volume ratio of ethanol in a solvothermal reaction system [100]. (Reprinted with permission from Ref. [100]. Copyright 2008, Elsevier)

to monitor the real time of the hydrothermal and solvothermal process, and the reaction usually proceeds without stirring, sometimes leading to the incomplete reaction and irregularly arranged product. Due to the fact that a variety of organic solvents can be used in the solvothermal method, it is easier to control the crystalline and morphology of the products than the hydrothermal method. Therefore, we can foresee that the solvothermal method has better application prospects.

### *6.3.2 Microemulsion-Mediated Solvothermal Method*

The method of microemulsion usually contains two processes. Firstly, two immiscible solvents divided into many micro-reactors (microbubbles) with the help of the surfactants form emulsion, in which nanomaterials are obtained through nucleation, coalescence, agglomeration, and heat treatment process in the oil-in-water or water-in-oil microbubbles. The reactants of immiscible solvents are well dispersed, and a uniform nucleation limited in the micro-reactors occurs. Therefore, the particle size and stability of the nanomaterials can be well controlled. Compared with other traditional synthesis methods, the microemulsion method has shown obvious advantages in terms of the preparation of nanomaterials with perfect monodispersity and interfacial properties. Moreover, this method is a very versatile technique which allows the synthesis of a great variety of nanomaterials by combining with other techniques. Recently, the microemulsion-mediated solvothermal method, which is named for the combination of the microemulsion method with solvothermal method, has been used to the preparation of the mixed-phase $TiO_2$ nanomaterials [66, 101, 102].

Yan et al. [66] fabricated anatase/rutile mixed-phase $TiO_2$ crystal through the combination of microemulsion and solvothermal method, using tert-octylphenoxypolyethoxyethanol (Triton X-100) as the surfactant, n-hexanol as the co-surfactant, and cyclohexane as the continuous oil phase. Tetrabutyl titanate and $(NH_4)_2SO_4$ were completely dissolved in the hydrochloric acid to serve as the

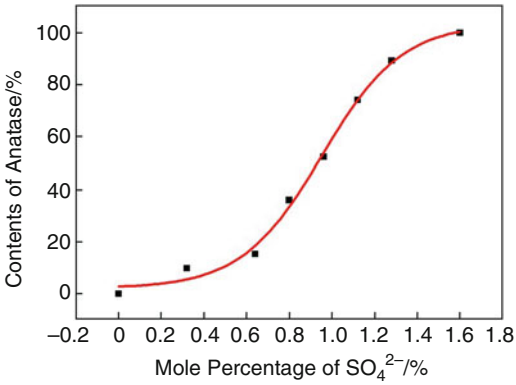


**Fig. 6.5** Relationship between the contents of anatase in the product and the mole percentage of $SO_4^{2-}$ in the microemulsion-mediated hydrothermal reaction system [66]. (Reprinted with permission from Ref. [66]. Copyright 2005, American Chemical Society)

aqueous phase. Then the aqueous phase was added dropwise to the oil phase to form a clear microemulsion. After that, the obtained solution was solvothermally treated below 120 °C for 13 h to produce the mixed-phase $TiO_2$. The surface area of the resultant product is about 86~169 $m^2/g$. Besides grain size of anatase is 15 nm and that of rutile is about 10 nm. Their results showed that the adjustment of $SO_4^{2-}$ concentration has obvious influence on the content of anatase in the mixed-phase $TiO_2$ (Fig. 6.5). With the increase of $SO_4^{2-}$ concentration, the anatase content in the mixed-phase $TiO_2$ increased. Different polymorphs can be achieved by affecting the polycondensation of $TiO_6$ octahedra with $SO_4^{2-}$ (Fig. 6.6a). During the hydrothermal reaction process, the $SO_4^{2-}$ interacts with the hydroxy groups on the surface of $TiO_6$ octahedra, forming hydrogen bonds (Fig. 6.6b). Because of the steric effect of $SO_4^{2-}$, the polycondensation of the octahedron with $SO_4^{2-}$ and another octahedron along the converse direction results in the decrease of the repulsion (Fig. 6.6c), and the orientation of the third octahedron is more conducive to form an anatase nucleus (Fig. 6.6d). When the concentration of $SO_4^{2-}$ is low, a rutile structure can be easily formed for the sake of the lowest free energy in the system. Therefore, controlled adjustment of anatase content in mixed-phase $TiO_2$ can be achieved by changing the concentration of $SO_4^{2-}$. In the same oil-phase system, Zhang et al. [102] synthesized mixed-phase $TiO_2$ crystal in different ratio of anatase and rutile content by the microemulsion-mediated solvothermal method. In the reaction system, a mixture of $TiCl_3$, urea, and hydrochloric acid solution was used as the aqueous phase. The results showed that anatase content in the mixed-phase $TiO_2$ increased with urea concentration increasing. The hydrochloric acid in the reaction solution served as an inhibitor to the generation of anatase, promoting the formation of rutile phase. Because $TiO_6$ octahedra polycondensed in chain to form a rutile structure was in accordance with the minimum energy principle, $Cl^-$ and $SO_4^{2-}$ had different influence on the formation of $TiO_2$ phases. A high concentration of $Cl^-$ with small radius and weak steric hindrance favored the formation of rutile $TiO_2$, while a high concentration of $SO_4^{2-}$ benefited to form anatase $TiO_2$.

Among the synthesis methods of mixed-phase $TiO_2$, the microemulsion-mediated solvothermal method is relatively complicated. However, the grain size of the

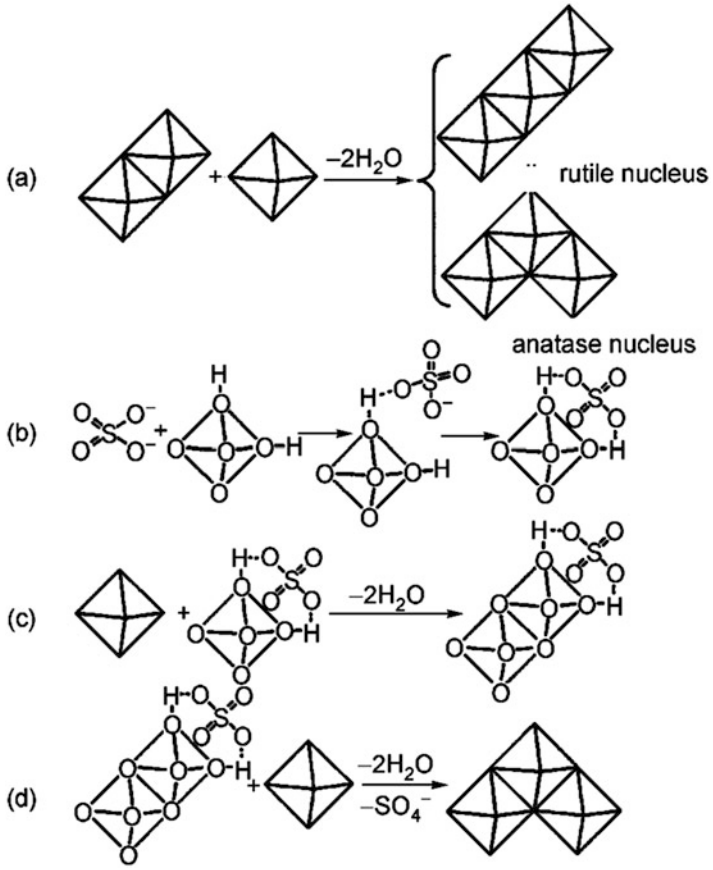


**Fig. 6.6** Proposed mechanism: (**a**) the orientation of the third octahedron determines the formation of rutile or an anatase nucleus; (**b**) interaction between $SO_4^{2-}$ anion and $TiO_6^{2-}$ octahedral hydroxyls; (**c**) two $TiO_6^{2-}$ octahedra share edge when $SO_4^{2-}$ is present; (**d**) the formation of anatase in the presence of $SO_4^{2-}$ [66]. (Reprinted with permission from Ref. [66]. Copyright 2005, American Chemical Society)

product is small, and the phases can be well controlled, which makes this method to have good prospects for development.

### *6.3.3 Sol–Gel Method*

Sol–gel method is a commonly used method for synthesis of amorphous and crystalline $TiO_2$ nanomaterials for the sake of its advantages such as processing at low temperature and the ability to prepare materials in various morphologies. Titanium alkoxides or titanium halides are usually used as the titanium precursor

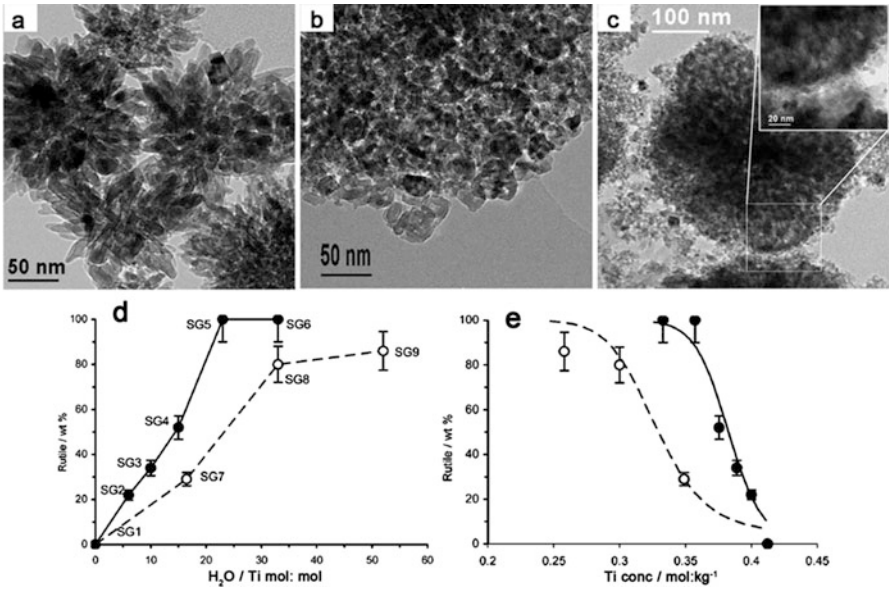


**Fig. 6.7** TEM images of (**a**) 100% rutile, (**b**) 100% anatase, and (**c**) mixed-phase $TiO_2$ with 48 wt % anatase and 52 wt % rutile; plots of rutile content (wt %) in the product (**d**) vs $H_2O$/Ti molar ratio (**e**) vs titanium concentration [52]. (Reprinted with permission from Ref. [52]. Copyright 2008, American Chemical Society)

in the sol–gel reaction system. Firstly, the hydrolysis of titanium precursor forms a sol. After aging the sol for a certain time, a three-dimensional cross-linked gel is obtained, and amorphous white powder is obtained by grinding the gel. Finally, crystallized $TiO_2$ is obtained by the treatment of the calcination at a certain high temperature.

Scotti et al. [52] prepared anatase/rutile mixed-phase $TiO_2$ crystal by a sol–gel method and studied the effects of HCl/Ti and $H_2O$/Ti molar ratio on the phase type of $TiO_2$ crystal. At first, $TiCl_4$ and triblock copolymer were dissolved in ethanol. Then water and HCl were added to adjust the pH of the solution, obtaining a sol. After aging the sol for 3–13 days, a gel was formed. After drying and calcination, mixed-phase $TiO_2$ crystals consisting of anatase and rutile in different content were obtained. In the products, pure rutile-phase $TiO_2$ (Fig. 6.7a) displayed chestnut burr aggregates of elongated nanocrystals in radial growing shape with average sizes of 10–20 nm in width and 100–200 nm in length. The pure anatase phase (Fig. 6.7b) showed aggregates of almost square-ended nanoparticles whose average sizes were 5–15 nm. The mixed-phase sample (Fig. 6.7c) was observed to possess two types of phases with the chestnut burr aggregates of rutile surrounded by the small anatase particles. Changing the $H_2O$/Ti ($r$w) and HCl/Ti ($r$a) molar ratios systematically can well control the phase content of the products. Results have proved that, in the titanium alkoxide or acidic titanium halide precursor solution, with the increase of $H_2O$ content, the concentration of $Ti^{4+}$ decreased, leading to the

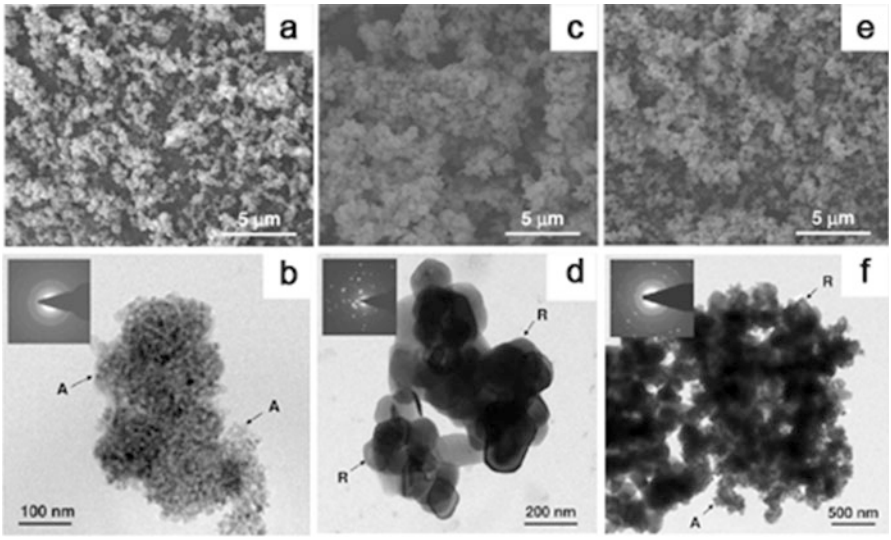


**Fig. 6.8** SEM and TEM images of (**a**, **b**) pure anatase, (**c**, **d**) pure rutile, and (**e**, **f**) mixed-phase $TiO_2$ with an optimum rutile content of 40 wt% prepared by the SMC method [103]. (Reprinted with permission from Ref. [103]. Copyright 2009, American Chemical Society)

decrease of the condensation reaction rate of $TiO_6$ octahedra to form rutile $TiO_2$ with better thermodynamically stability (Fig. 6.7d, e).

Mixed-phase $TiO_2$ crystals with small particles and high purity can be obtained by the sol–gel method, but the experimental procedure usually requires longtime aging, and the agglomeration of particles is easy to occur after high-temperature calcination, which may cause significant decrease of the photocatalytic activity.

### *6.3.4 Solvent Mixing and Calcination Method*

The solvent mixing and calcination method (SMC method) means to mix $TiO_2$ with different phases in a certain solvent at first and then to evaporate the solvent completely, finally followed by calcinations at high temperature in order to make a close contact among different crystal phases. Zachariah et al. [103] prepared anatase/rutile mixed-phase $TiO_2$ by the SMC method wherein anhydrous isopropanol was used as the solvent. According to the Scherrer equation, the crystalline calculated size of pure anatase was 10 nm, and the grain size of pure rutile was 40 nm. In the resultant mixed-phase $TiO_2$ containing 40% rutile, the size of anatase was 29 nm and that of rutile was 47 nm. From Fig. 6.8a, b, it could be observed that pure anatase consisted of small particles whose size was 100~150 nm. And as Fig. 6.8c, d shows, the particle size of pure rutile was 300~500 nm. The morphology of the mixed-phase $TiO_2$ nanomaterial was a mixture of anatase and rutile particles (Fig. 6.8c, f). From

the high-resolution transmission electron microscopy (HRTEM), the phase interface could be seen clearly, indicating a close interaction existing between the two phases. Bojinova et al. [104] synthesized an anatase/rutile mixed-phase $TiO_2$ by the SMC method using ethanol as the solvent. In the product, the grain size of anatase was 42 nm and that of rutile was 56 nm which are calculated according to the Scherrer formula. Liu et al. [105] used a layer-by-layer self-assembly technique to make the anatase small particles adsorbed onto rutile nanorods with assist of polystyrene sulfonate (PSS) as a medium, and finally the PSS was removed by calcination. The anatase content in the mixed-phase $TiO_2$ crystal could be controlled by adjusting the number of loading cycles.

The phase content of the mixed-phase $TiO_2$ can be regulated easily by using the SMC synthesis method. However, because the final calcination process requires high temperature, the $TiO_2$ is easy to agglomerate. In addition, it is usually difficult to obtain the mixed-phase $TiO_2$ with anatase and rutile mixing uniformly, causing products with many pure rutile aggregates as well as pure anatase aggregates. Therefore, the photocatalytic performance of the mixed-phase $TiO_2$ crystals produced by this method is limited.

### 6.3.5 *High-Temperature Calcination Method*

The high-temperature calcination method, which is mostly used to research the phase transition of $TiO_2$, is one of the earliest methods for the synthesis of mixed-phase $TiO_2$ [25].

Through the high-temperature calcination method, Nair et al. [106] succeeded in preparing the mixed-phase $TiO_2$ nanomaterials with different anatase and rutile contents. They firstly prepared small anatase particles by a sol–gel method followed by calcinating the anatase particles at elevated temperatures. It was found that the samples which were calcined at low temperatures ($T < 600$ °C) remained pure anatase phase. The phase transformation began at the temperature of 650 °C. When the calcination temperature was raised to 850 °C, the product converted to pure rutile. As calculated by the Scherrer formula, the grain sizes of anatase and rutile in the mixed-phase products were 33.66~51.48 nm and 45.2~60.6 nm, respectively. Figure 6.9 showed that the particle size of anatase was about 100 nm and that of rutile was about 200 nm, and the mixed-phase particle size was between the above two and increased with the increase of calcination temperature. The phase transformation includes nucleation and growth. However, there is some dispute on the concrete process. Gouma et al. [107] considered that the rutile firstly formed nuclear on the surface of anatase and then expanded to the bulk, while Zhang et al. [108] verified the phase transformation of anatase–rutile occurred in the bulk at first and then spread to the surface with the increase of calcination temperature via UV Raman spectroscopy. Figure 6.10 shows the phase's transformation.

The simple high-temperature calcination method can be used to obtain mixed-phase $TiO_2$ nanomaterials with perfect polymorphs and tunable phase content.

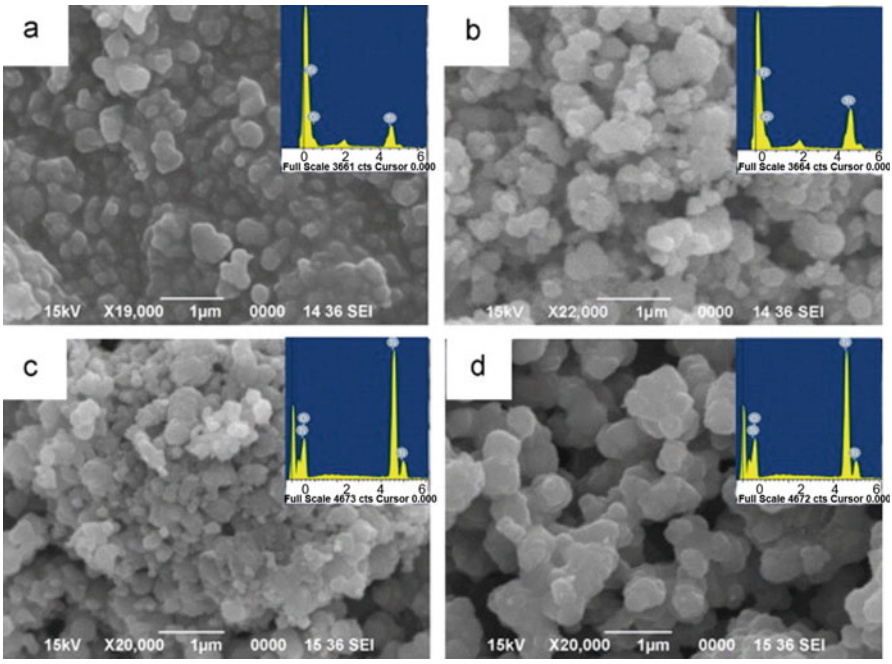


**Fig. 6.9** SEM and EDAX images of $TiO_2$ photocatalysts calcined at different temperature: (**a**) 600 °C, (**b**) 700 °C, (**c**) 750 °C, and (**d**) 800 °C [106]. (Reprinted with permission from Ref. [106]. Copyright 2011, Elsevier)

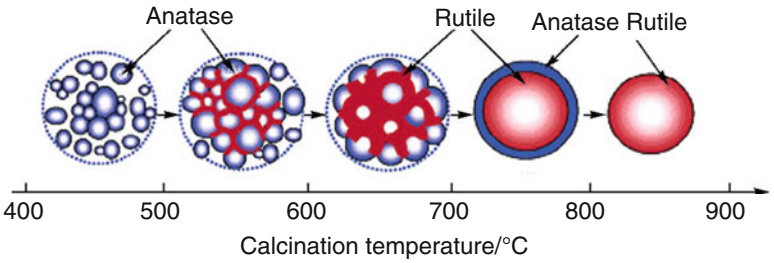


**Fig. 6.10** Proposed schemes for the phase transformation of titania with increasing calcination temperature [108]. (Reprinted with permission from Ref. [108]. Copyright 2006, American Chemical Society)

However, it is easy to agglomerate in the process of calcination, and the particles size of product is large, resulting in the decrease of the photocatalytic activity.

Generally speaking, both the SMC method and the high-temperature calcination method require a high temperature to form the mixed-phase $TiO_2$ or close contact between different crystalline forms. The electron micrographs and XRD results showed that the grain size of crystal after calcination at high temperature is significantly larger than that of mixed-phase $TiO_2$ crystals obtained by the in situ method.

**Table 6.2** The photocatalytic reaction rate constants of mixed-phase $TiO_2$ synthesized by different methods

| Synthesis method | Rate constants/$min^{-1}$ | References |
|---|---|---|
| Hydrothermal method | 0.019 | [53] |
| Sol–gel method | 2.400 | [51] |
| Microemulsion-mediated | 0.030 | [75] |
| Solvothermal method | | |
| SMC method | 0.023 | [77] |
| Calcination method | 0.003 | [79] |

Besides, the agglomeration of $TiO_2$ product is also serious. All of the before mentioned can easily decrease the photocatalytic activity of mixed-phase $TiO_2$. Therefore, in recent years, these methods are used less and less.

The photocatalytic reaction rate constants of mixed-phase $TiO_2$ crystals synthesized by different methods are summarized in Table 6.2. From this table, we can see that the reaction rate of $TiO_2$ by prepared in situ methods, such as the sol–gel method and microemulsion-mediated hydrothermal method, is usually higher than the high-temperature calcination method or SMC method. This is because the latter requires high-temperature calcination, leading to larger particle size and serious agglomeration that decrease the contact area with the degradation target and further impact the photocatalytic activity. However, the photocatalytic reaction rate of mixed-phase $TiO_2$ prepared by Zheng et al. [54] was low, which may be attributed to the high-temperature calcination which leads to a hollow structure and decreases the specific surface area, thus causing low photocatalytic activity. Photocatalytic activities of mixed-phase $TiO_2$ prepared on different conditions are also influenced by many other factors such as product morphology, particle size, and crystal proportion.

Apart from the commonly used approaches mentioned above, there are some new preparation methods of mixed-phase $TiO_2$, such as the microwave-heating method [109]. The particle size of $TiO_2$ prepared by this method is smaller than that synthesized by heating with an oil bath. With the development of new technologies, we can foresee that there will be more new methods for preparing mixed-phase $TiO_2$.

## 6.4 Applications of Mixed-Phase $TiO_2$ in Photocatalysis

### *6.4.1 Photocatalytic Hydrogen Production*

Faced with the increasingly serious energy crisis, hydrogen has been widely recognized as an ideal energy source to replace a significant fraction of fossil fuels. However, nowadays the $H_2$ source demanded is mostly produced from fossil feedstock, mainly via steam reforming of methane. It is therefore necessary to develop sustainable methods for hydrogen production. Among them, the photocatalytic hydrogen production is one of the most promising technologies,

which possesses various advantages, such as sustainability of the primary energy source (the solar light), the renewability of the starting feedstock, as well as the possible production of by-products with a high added value [110]. Due to the merits of $TiO_2$ such as nontoxicity, relatively cheap cost, easy to prepare, and excellent stability under the reaction conditions, it is the most investigated photocatalyst for $H_2$ production. However, the present solar-to-hydrogen energy conversion efficiency of $TiO_2$ is not high enough for the applications in commercial production. The rapid recombination of photo-generated electron–hole pairs of the materials, backward reaction, and the poor utilization of visible light hinder the practical applications. In order to solve the problems mentioned above, many researchers have been conducting studies concentrated on an emphasis to develop effective remediation methods like modification of $TiO_2$ by noble metal loading, metal ion doping, anion doping, dye sensitization, composite semiconductor, and metal ion implantation. In addition, mixed-phase $TiO_2$ has also been investigated for hydrogen production [91, 110–114], since mixed-phase $TiO_2$ nanomaterials demonstrated higher performances than the correspondent monophasic systems in many photocatalytic processes.

Chen et al. [91] successfully prepared pure anatase nanoparticles, pure brookite nanoplates, and two-phase anatase/brookite $TiO_2$ photocatalysts by a simple hydrothermal method. The photocatalytic activity of the as-synthesized catalysts for hydrogen production was studied in methanol solution. Their experimental results have shown that the photocatalytic activity of the two-phase anatase/brookite $TiO_2$ was higher compared with that of pure brookite nanoplates and pure anatase nanoparticles, as shown in Fig. 6.11. Moreover, in comparison with the highly active two-phase commercial P25, the synthesized two-phase anatase/brookite $TiO_2$ was 220% more active when measured by the $H_2$ yield per unit area of the photocatalyst surface. Similar results were achieved by Montini et al. [111]. They also prepared the

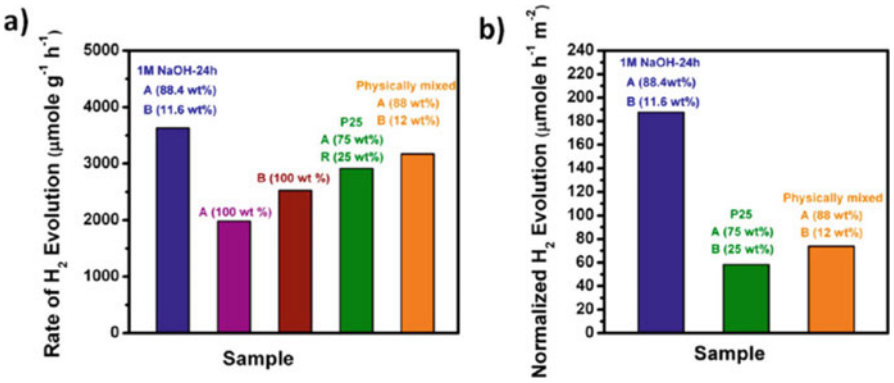


**Fig. 6.11** Hydrogen evolved per gram of photocatalyst per hour under UV−vis irradiation in aqueous methanol solution over 0.3 wt % Pt-loaded photocatalysts. A, B, and R stand for anatase, brookite, and rutile, respectively [91]. (Reprinted with permission from Ref. [91]. Copyright 2013, American Chemical Society)

mixed-phase $TiO_2$ of anatase/brookite via hydrothermal treatments. Compared with a reference $TiO_2$ prepared by conventional sol–gel synthesis, the anatase/brookite nanocomposites which are obtained by hydrothermal method showed the higher photocatalytic activity for producing $H_2$. Furthermore, they found that the anatase/brookite ratio in the nanocomposite had a great influence on the photocatalytic activity in $H_2$ production.

Apart from the research applying mixed-phase anatase/brookite $TiO_2$ as the photocatalyst to produce hydrogen, a great deal of research on the mixed-phase anatase/rutile $TiO_2$ has also been done. Li et al. [112] fabricated photocatalysts with a tuned anatase/rutile structure by calcination of commercial P25 at different temperatures and investigated their photocatalytic activity for hydrogen production through photocatalytic biomass reforming. Surprisingly, it was found that compared with P25 without any treatment, the photocatalytic performance of the thermal-treated P25 for hydrogen production is better. The overall photocatalytic activity for hydrogen production on thermal-treated P25 had a dramatic improvement of three to five times. It was proposed that the anatase/rutile junction structure was mainly responsible for the enhanced photocatalytic performance. The research work implied that the photocatalytic ability of $TiO_2$ could be further improved by elaborately designing the anatase/rutile structure. Amal et al. [113] obtained the similar conclusions. They did a systematical study on photocatalytic $H_2$ evolution using mixed-phase $TiO_2$ as a function of anatase and rutile phase compositions with methanol as hole scavengers. The $TiO_2$ nanomaterials they prepared contain 4–95 mol % anatase, with the remaining being rutile. Synergistic effects on $H_2$ evolution were observed for a wide range of anatase contents, from 13 to 79 mol %, while due to insufficient physical contact, no synergistic effect was observed for the sample obtained by mixing anatase and rutile particles physically. Recently, in addition to the above research on particulate $TiO_2$ (Fig. 6.12a, b), Yu et al. [114] prepared a kind of anatase/rutile $TiO_2$ nanofiber photocatalyst (Fig. 6.12b, c). The enhanced photocatalytic performance for $H_2$ production was also observed in the synthesized anatase/rutile composite nanofibers. The product with 45 wt.% rutile phase and 55 wt.% anatase phase exhibited the highest photocatalytic activity with the $H_2$ production rate of 324 mmol $h^{-1}$ and the apparent QE of 20.9% at 365 nm.

Though the research on the mixed-phase $TiO_2$ of anatase/rutile generally demonstrated that the combination of the two phases favored the photocatalytic hydrogen production efficiency, the low utilization rate of visible light still remains as a big limit for its practical application. The relatively narrow bandgap of rutile extends some visible light absorption to some extent. However, this is not enough for $TiO_2$ photocatalyst to apply in the practical applications. Researchers have made great efforts on to expand the visible light absorption of the mixed-phase $TiO_2$ crystals. Keller et al. [115] reported Au-modified anatase/rutile mixed-phase $TiO_2$ photocatalyst (Fig. 6.13) for hydrogen production. The light absorption of the sample with and without Au deposition was investigated via UV–vis light absorption spectra. Before the Au deposition, the catalyst with rutile phase whose content was higher than that of P25 exhibited more light absorption extended up to 550 nm, but its intensity is relatively low. After Au deposition, the samples showed an obvious

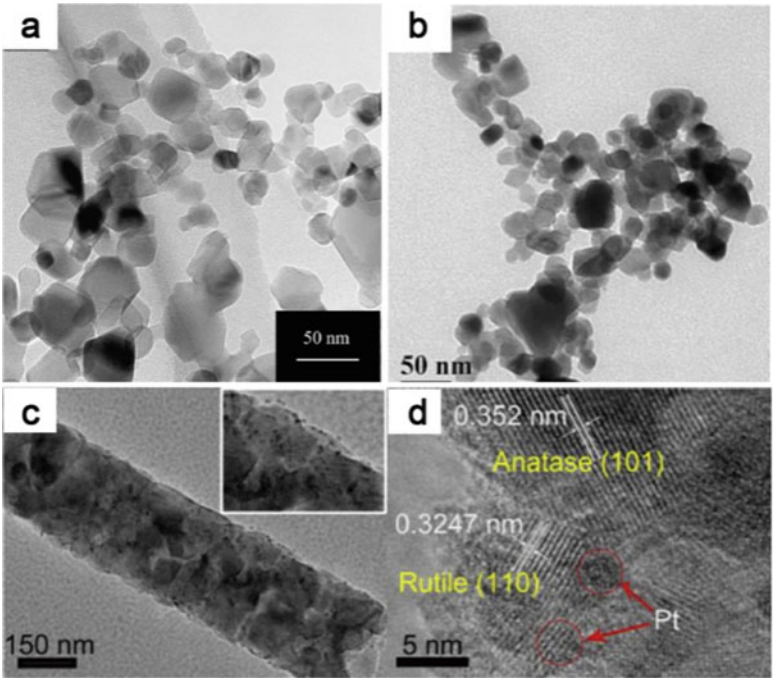


**Fig. 6.12** (**a** and **b**) TEM images of particulate anatase and rutile phase $TiO_2$; (**c** and **d**) TEM and HRTEM images of fibrous anatase and rutile $TiO_2$ [112]. (Reprinted with permission from Ref. [112]. Copyright 2011, Elsevier)

modification of the light absorption properties, yielding an additional absorption band around 550 nm. It could be attributed to a plasmon resonance phenomenon [116] owing to collective oscillations of the conduction electrons located on the 6s orbital of Au and induced by the incident electromagnetic wave. In addition to this plasmon absorption, Au deposition also benefited to shift the absorption spectrum of $TiO_2$ photocatalysts deeper into the visible light range of 380–450 nm. This enhanced light absorption in the visible region was demonstrated to contribute to the improved photocatalytic performance of $TiO_2$ for the hydrogen production under the irradiation of simulated solar light. Furthermore, they pointed out that there were various factors which were crucial to improve $H_2$ evolution efficiency: (i) the surface and the crystallographic porosity properties of the $TiO_2$ anatase/rutile photocatalyst, (ii) the anatase/rutile ratio, (iii) the amount and nature of the metallic cocatalyst, (iv) the metal–support interactions, and (v) the relative content of sacrificial reagent. After studying the influence of these different factors in depth, they optimized the experimental conditions, obtaining the important $H_2$ production efficiency up to120 μmol $min^{-1}$ over days without deactivation and with very low amounts of sacrificial reagent.

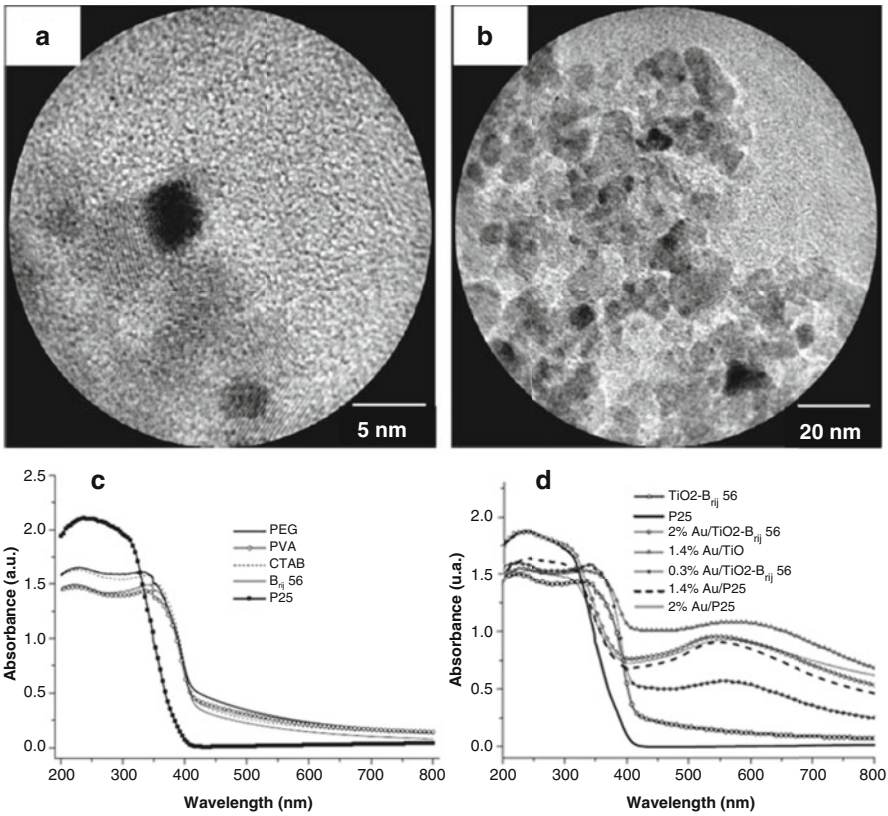


**Fig. 6.13** (**a, b**) TEM images of mixed-phase $TiO_2$ photocatalyst deposited Au; (**c**) Light absorption properties of mixed-phase $TiO_2$ without and with Au deposition [115]. (Reprinted with permission from Ref. [115]. Copyright, 2010 Elsevier)

### *6.4.2 Photocatalytic Reduction of $CO_2$ with Water on Mixed-Phase $TiO_2$*

As we know, $CO_2$ is the main cause of the greenhouse effect, which leads to global warming. Meanwhile, based on the fact that $CO_2$ can be converted into various useful chemical compounds and fuels such as $CH_4$, $CH_3OH$, and HCOOH, it is also a promising carbon resource. Therefore, in order to reduce the emissions of $CO_2$ and to obtain a sustainable energy, many kinds of novel materials and new technologies have been developed to convert $CO_2$. Besides the methods of solar thermochemical conversion as well as electrochemical reduction of $CO_2$, solar-activated photocatalytic reduction of $CO_2$ with water by $TiO_2$ at atmospheric pressure and room temperature has attracted much attention due to its "green chemistry" and relatively low cost.

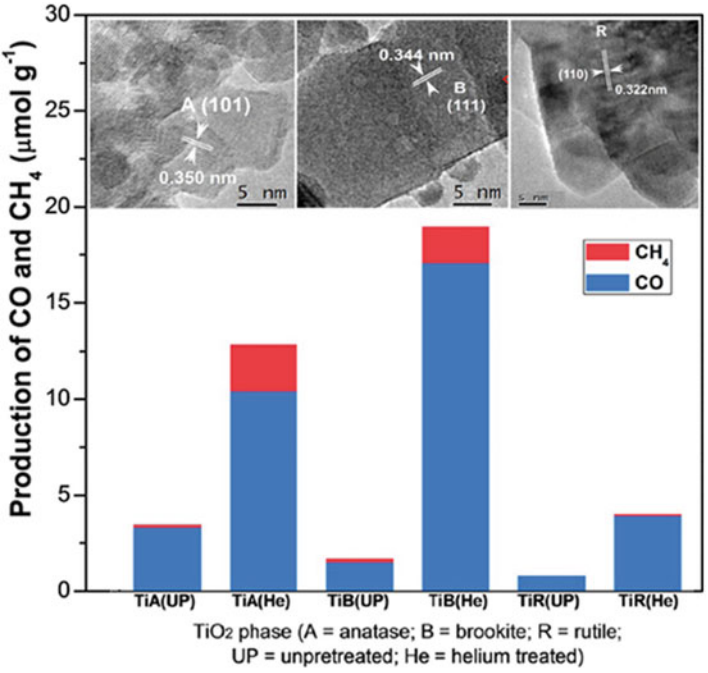


**Fig. 6.14** The top figure are TEM images of different $TiO_2$ crystals: anatase, brookite, and rutile (from left to right). The bottom figure is the production of CO and $CH_4$ with the three different $TiO_2$ polymorphs [117]. (Reprinted with permission from Ref. [117]. Copyright 2012, American Chemical Society)

During the process of $CO_2$ photocatalytic reduction with $H_2O$ by $TiO_2$, the irradiation of solar light activates the generation of electron–hole pairs in $TiO_2$ nanomaterials. The excited electrons in the conduction band (CB) of $TiO_2$ photocatalyst migrate to the surface to reduce $CO_2$. Meanwhile, the holes left in the valence band (VB) of $TiO_2$ can oxidize $H_2O$ into $O_2$.

It has been proved that the above photocatalytic process had a close relation with the phase type of $TiO_2$. Li et al. [117] investigated the $CO_2$ photoreduction with water vapor on three types of $TiO_2$ nanocrystal polymorphs (anatase, rutile, and brookite). The results showed that the photocatalytic reduction activity of different-phase $TiO_2$ nanomaterials follows the order: anatase > brookite > rutile. Because of the fast $e^-$ and $h^+$ recombination in rutile, it showed the least photocatalytic activity. Besides, the photoreduction activity of the $TiO_2$ catalysts with a helium treatment was investigated. The photoreduction data indicated that photocatalysts with a helium treatment were more active than the samples without a helium treatment. And the photocatalytic activity for production of CO and $CH_4$ from the photoreduction of $CO_2$ followed the order, brookite > anatase > rutile (Fig. 6.14), where brookite showed the highest photocatalytic activity. Thus their study also implied that the brookite phase is a promising material for the photoreduction of $CO_2$; they

performed further research on this topic, including the study on brookite-containing mixed-phase $TiO_2$. They prepared bicrystalline anatase/brookite $TiO_2$ photocatalysts via a hydrothermal method [118]. The as-prepared anatase/brookite $TiO_2$ was also applied for $CO_2$ photoreduction with water vapor for the production of CO and $CH_4$. Compared with those of pure anatase, pure brookite, and a commercial anatase/rutile $TiO_2$ (P25), the photocatalytic activities of bicrystalline anatase/brookite $TiO_2$ were better. Wherein, the bicrystalline mixture with a composition of 75% anatase and 25% brookite showed the best photocatalytic performance, whose photocatalytic activity was nearly twice as high as that of 100% anatase (A100) and three times as high as that of pure brookite (B100) $TiO_2$. Because pure anatase A100 possessed the largest specific surface area and the smallest bandgap among three types of $TiO_2$ phases, the higher photocatalytic activity of bicrystalline anatase/brookite was very likely ascribed to the interactions between the anatase and brookite nanocrystals. In addition, the result that the anatase-rich bicrystalline anatase/brookite mixtures were superior to anatase/rutile mixture P25 which indicated the interaction between anatase and brookite of as-prepared mixed-phase $TiO_2$ seems to be more effective than that of P25 in the photoreduction of $CO_2$.

### *6.4.3 Photocatalytic Degradation of Organic Pollutants on Mixed-Phase $TiO_2$*

In 1977, S. N. Frank and A. J. Bard reported that $TiO_2$ could effectively decompose the cyanide in aqueous medium under sunlight for the first time [119]. From then on, the application of $TiO_2$ for photocatalytic degradation of organic pollutants such as organic dyes has raised wide attention due to its effectiveness in degrading and mineralizing the toxic, bio-refractory, and highly concentrated organic compounds as well as the possibility of utilizing the solar ultraviolet and visible light spectrum. Owing to the superiority that mixed-phase $TiO_2$ usually exhibit better photocatalytic activity than single-phase $TiO_2$, $TiO_2$ nanomaterials consisting of different phases have also been widely used to degrade organic pollutants.

There have been many studies on the photocatalytic degradation of organic dyes using mixed-phase $TiO_2$ as photocatalyst. For example, under simulated solar light irradiation, the degradation of methyl blue (MB) was carried out in the aqueous solution by anatase/rutile $TiO_2$ heterojunction nanoflowers [120]. It was found that 72% of MB could be degraded in 120 min in the presence of the mixed-phase photocatalyst prepared in optimized experimental conditions, while only 30% of MB could be degraded in the solution with 100% anatase. Besides, the $TiO_2$ nanoflower photocatalysts showed excellent stability after nine cycles under the same conditions, suggesting that the mixed-phase anatase/rutile $TiO_2$ heterojunction nanoflower materials have great potential for the future photodegradation of practical dye wastewater. Since high surface area favors high photocatalytic activity, mesoporous mixed-phase anatase/rutile $TiO_2$ was also fabricated [121] (Fig. 6.15a) to apply for

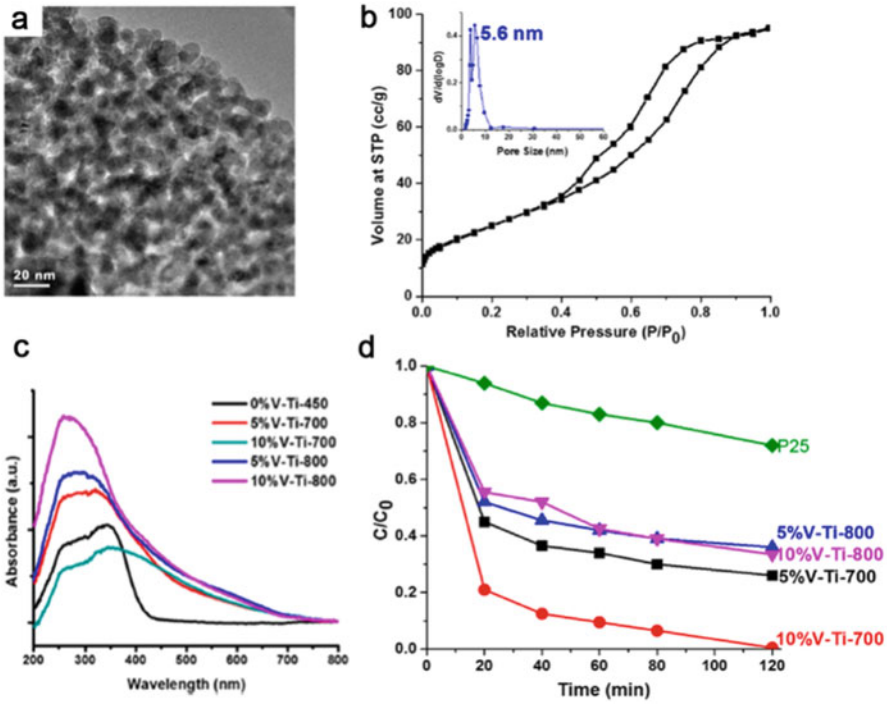


**Fig. 6.15** (**a**) TEM image of mesoporous anatase/rutile mixed-phase $TiO_2$ (10%V-Ti-700); (**b**) $N_2$ sorption isotherms of 10%V-Ti-700. The inset, the BJH desorption pore-size distributions; (**c**) DR UV−vis spectra for various vanadium-doped mixed-phase $TiO_2$; (**d**) photocatalytic decomposition experiments of 100 mL, $10^{-4}$ MB dye under visible light in 2 h by using 100 mg of 5% V-Ti-700, 10%V-Ti-700, 5%V-Ti-800, 10%V-Ti-800, and P25 samples, respectively [121]. (Reprinted with permission from Ref. [121]. Copyright 2014, American Chemical Society)

the photocatalytic degradation of MB. The optimum mesoporous photocatalyst (10%V-Ti-700) in situ doped with vanadium with the surface area up to 94 $m^2$ $g^{-1}$ and an average pore size of 5.6 nm (Fig. 6.15b) exhibited higher photocatalytic activity under visible light than that of the commercial P25 (Fig. 6.15d), in which the vanadium doping helped to extend the absorption of $TiO_2$ to the visible light region (>400 nm) (Fig. 6.15c). It was concluded that the high surface area, the mixed-phase effect, and the vanadium doping altogether contributed to the enhanced photocatalytic performance of the mesoporous mixed-phase anatase/rutile $TiO_2$.

In addition to the anatase/rutile $TiO_2$, many studies on brookite/rutile $TiO_2$ for the photodegradation of dyes have been done, such as Zhang et al.'s [81] work. They prepared mixed-phase $TiO_2$ photocatalysts with a tunable brookite-to-rutile ratio through a facile controllable one-pot hydrothermal method. And the photocatalytic performance of the as-prepared $TiO_2$ nanocrystals was tested in the degradation of Rhodamine B under the simulated solar light. Compared with the samples with other brookite-to-rutile ratios, the mixed-phase $TiO_2$ nanocrystals with 38% brookite and

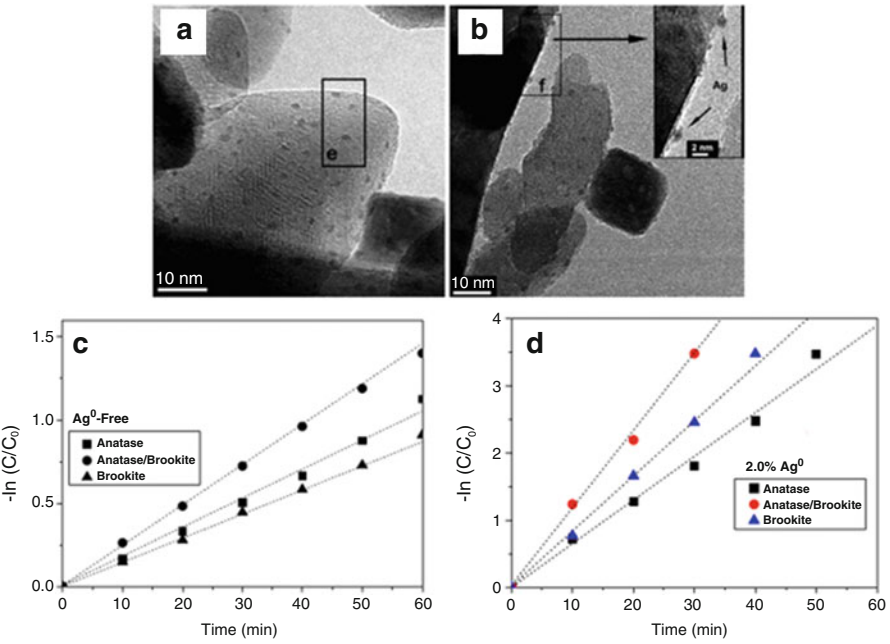


**Fig. 6.16** (**a** and **b**) TEM images of 2.0% $Ag^0$–$TiO_2$ (brookite/anatase); (**c**) photocatalytic degradation of MO with Ag-free and 2.0% $Ag^0$-loaded (**d**) $TiO_2$ photocatalysts with different crystal phase composition under UV irradiation [55]. (Reprinted with permission from Ref. [55]. Copyright 2012, Elsevier)

62% rutile showed the highest photocatalytic activity, which was about six times that of the commercial P25 catalysts. Recently, Chen et al. [55] grew anatase grains on the surface of brookite petals to form a brookite/anatase $TiO_2$ hybrid, which appeared to have superior photocatalytic activity to the single-phase $TiO_2$ during the degradation of methyl orange (MO) as well as 2,4-dichlorophenol (2,4-DCP). The hybrid consisting of 60% brookite and 40% anatase exhibited the highest activity, whose degradation rate constants are 2.27 and 1.80 times higher than that of the corresponding physically mixed brookite/anatase $TiO_2$ for the photodegradation of MO and 2,4-DCP, respectively. Following this study, Ag was utilized to further modify the brookite/anatase composite [122]. $Ag^0$ clusters, which possessed an average diameter of ca. 1.5 nm, formed on the surface of the mixed-phase $TiO_2$ (Fig. 6.16a, b). The photocatalytic performance of the as-prepared photocatalysts was examined for the degradation of methyl orange (MO). As shown in Fig. 6.16d, the photodegradation reaction rate constant of $Ag^0$-loaded brookite/anatase composite was higher than that of the pure anatase and brookite, indicating an improved photocatalytic activity. Besides, it was found that the $Ag^0$-loaded mixed-phase $TiO_2$ photocatalysts showed better photocatalytic performance than that of Ag-free sample by comparing the results in Fig. 6.16c, d. The enhanced photocatalytic reactivity could be ascribed to the significant improvement in the

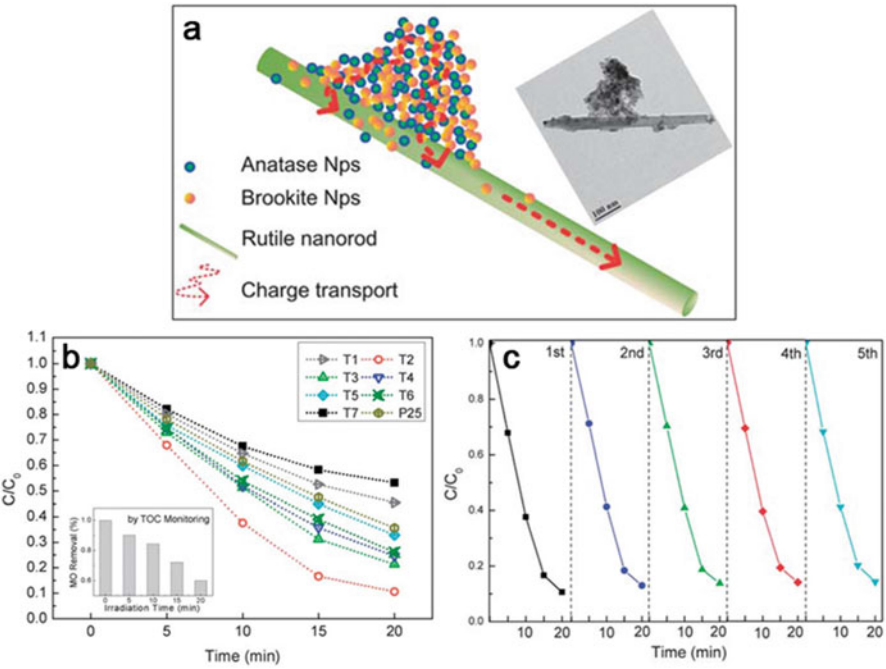


**Fig. 6.17** (**a**) Scheme of the brookite/anatase/rutile nanocomposites; inset, TEM image of as-prepared composite; (**b**) photocatalytic degradation of MO solution by using the brookite/anatase/rutile nanocomposites prepared with various reagent ingredients, and the inset shows the removal of MO monitored by TOC with the sample T2; (**c**) cycling degradation curves of the brookite/anatase/rutile triphasic nanocomposites (sample T2) [123]. (Reprinted with permission from ref. [123]. Copyright 2012, Royal Society of Chemistry)

separation of the photo-generated electrons and holes, which was caused by two aspects: (1) synergistic effect of anatase and brookite in the composite and (2) the Schottky barrier at the interface of $TiO_2$ and $Ag^0$.

While most research focused on photocatalytic degradation properties of biphasic $TiO_2$ photocatalysts, Que. et al. [123] prepared brookite/anatase/rutile triphasic $TiO_2$ composite as the photocatalysts for degradation of MO. Their experimental results indicated that in the brookite/anatase/rutile coexisting nanomaterials, the brookite and anatase phases were crystallized into irregular nanoparticles with diameter sizes of less than 20 nm, whereas the rutile phase was crystallized into single-crystalline nanorods about 20 nm in diameter and 100–500 nm in length, as Fig. 6.17a shows. Under irradiation of UV light, the as-prepared triphasic $TiO_2$ photocatalyst was demonstrated to possess better photocatalytic activity during degradation of MO than the biphasic commercial P25. The catalyst with 29.9% anatase, 27.9% brookite, and 42.2% rutile (referred as T2) had the highest photocatalytic activity, removing 90% of MO in 20 min (Fig. 6.17b). The photodegradation rate constant k of this sample was 0.10180 $min^{-1}$, which is nearly twice higher than that of P25

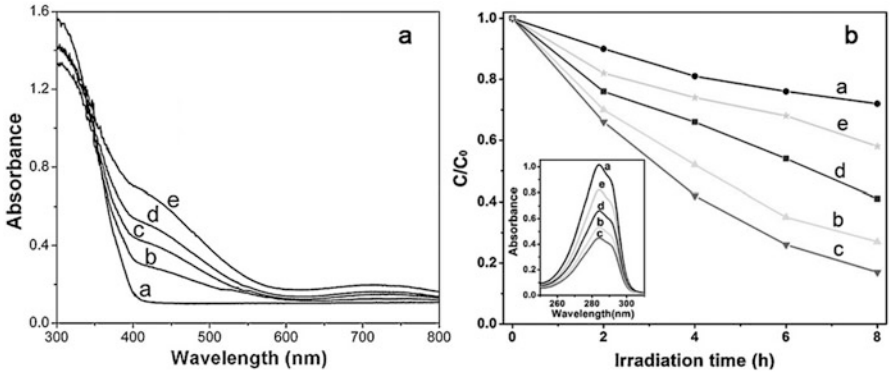


**Fig. 6.18** (**a**) UV–vis DRS and (**b**) photocatalytic degradation curves of 2,4-DCP over $TiO_2$ without doping and different Cr-$TiO_2$ samples under visible light irradiation: (a) $TiO_2$ without doping, (b) 0.5% Cr-$TiO_2$, (c) 1% Cr-$TiO_2$, (d) 2% Cr-$TiO_2$, and (e) 5% Cr-$TiO_2$. The inset is the absorption spectra of 2,4-DCP over different as-prepared photocatalysts after visible light irradiation for 8 h [126]. (Reprinted with permission from ref. [126]. Copyright 2012, Elsevier

($k = 0.05397\ min^{-1}$). In addition, as shown in Fig. 6.17c, the photocatalytic activity of the best photocatalyst T2 showed only a slight loss after five recycles, indicating a good stability of the triphasic $TiO_2$ photocatalyst in the degradation process. Similarly, Shao et al. also developed brookite/anatase/rutile coexisting $TiO_2$, and the as-prepared photocatalyst was demonstrated to show excellent photocatalytic performance for the degradation of methylene blue solutions.

Apart from dyes, some other organic compounds such as phenol and benzyl alcohol have also been used as the target pollutants in the mixed-phase $TiO_2$ photocatalysis system. Because phenol as well as its derivatives, as one type of primary pollutants, is able to do harm to organisms at low concentrations, many studies on the photodegradation of phenol have been widely carried out [124]. Lu et al. [125] synthesized a series of mixed-phase $TiO_2$ samples with different anatase-to-rutile ratios and studied the effects of crystal phase in photocatalytic oxidation of phenol aqueous solution. They found that the photocatalysts with higher anatase-to-rutile ratios showed higher photocatalytic activities for phenol degradation. Tian et al. [126] reported Cr-doped anatase/rutile bicrystalline phase $TiO_2$ (Cr-$TiO_2$) nanoparticles for the photocatalytic degradation of 2,4-dichlorophenol (2,4-DCP). Their experimental results showed that $Cr^{3+}$ doping could not only effectively extend the visible light response of $TiO_2$ nanomaterials (Fig. 6.18a) but also enhance the anatase-to-rutile transformation. The photocatalytic activities of different Cr-$TiO_2$ photocatalysts for the photocatalytic degradation of 2,4-dichlorophenol (2,4-DCP) were evaluated under the irradiation of visible light (Fig. 6.18b). It is found that appropriate $Cr^{3+}$ doping can remarkably enhance the visible light photocatalytic activity of $TiO_2$, which is ascribed to improving the response of visible light as well as suitable anatase-to-rutile ratio. In addition, excess $Cr^{3+}$ doping is unfavorable for improving visible light photocatalytic activity, because of the formation of $Cr_2O_3$ clusters and the excessive rutile content.

## 6.5 Mechanism of the Enhanced Photocatalytic Activities by the Mixed-Phase $TiO_2$ Photocatalysis

Generally, most of the photo-generated electrons and holes in the single-phase $TiO_2$ will recombine, and only a small amount of the excitons can migrate to the surface to participate in the oxidation–reduction reactions with absorbed molecules, causing relatively low photocatalytic efficiency. In 1991, Bickley et al. [76] first put forward the mechanism of enhanced photocatalytic activity of P25 consisting of 80% anatase and 20% rutile. They demonstrated that the mixed-phase structure of P25 is an anatase nanostructure coated with a layer of rutile film via TEM. Compared with any other single-phase $TiO_2$ photocatalyst, the evaluation results showed that the photocatalytic activity of the mixed-phase $TiO_2$ was significantly improved. Because of the different bandgaps, a bending band was formed on the interface of anatase and rutile, as shown in Fig. 6.19. Under light irradiation, the photo-generated electrons migrated from rutile phase to anatase phase, while the holes migrated from anatase phase to rutile phase; thus the electrons and holes could be separated effectively, leading to a high photocatalytic activity of the mixed-phase P25. Meanwhile, they proposed that the mechanism of the improved photocatalytic performance of mixed-phase $TiO_2$ was actually more complex and required further study. Subsequently, much research work on the mobility direction of the photo-generated carriers, the molecular dynamic characterizations of the mixed-phase interface [76], the band structure of mixed-phase $TiO_2$ photocatalysts [127, 128], and the suitable phase proportion in the mixed-phase crystal $TiO_2$ has been done to study the mechanism in depth.

In 1995, through observing the mixed-phase crystal structure in P25 via X-ray diffraction (XRD) and high-resolution transmission electron microscopy (HRTEM)

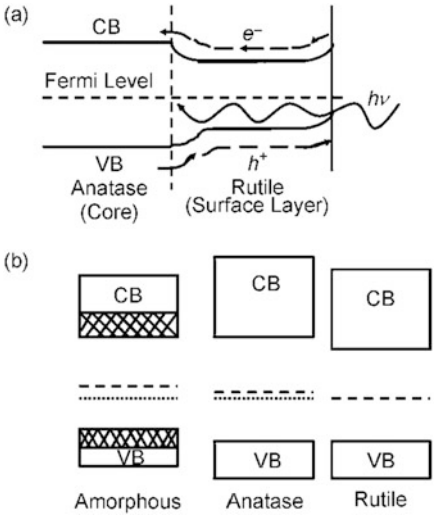


**Fig. 6.19** Schematic diagram of P25 band structure [76]. (Reprinted with permission from Ref. [76]. Copyright 1991, Elsevier)

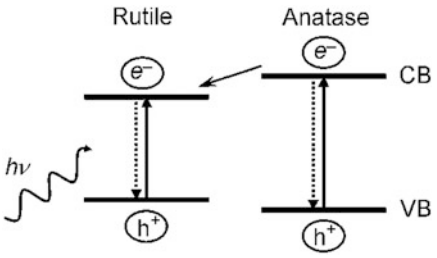


**Fig. 6.20** A proposed schematic diagram showing the migration behavior of the electron transferring from anatase to rutile [132, 133]. (Reprinted with permission from Ref. [132]. Copyright 2002, Wiley Online Library. Reprinted with permission from Ref. [133]. Copyright 2007, Elsevier)

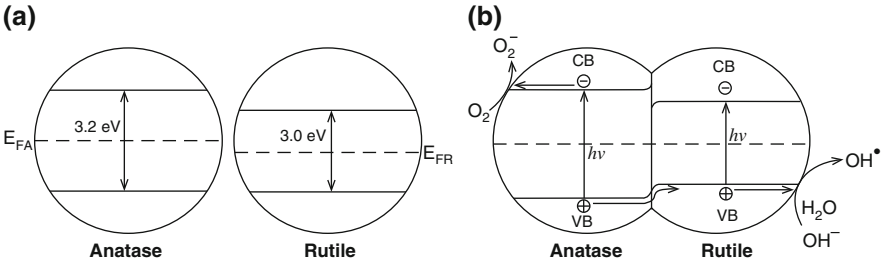


**Fig. 6.21** (**a**) Band structure of anatase and rutile before they contact each other; (**b**) band structure and the separation of photo-generated excitons after anatase and rutile contact each other [134]. (Reprinted with permission from Ref. [134]. Copyright 2003 American Chemical Society)

techniques, Datye et al. [129] put forth distinguishing views against Bickley et al. [76]. The characterization results showed that the mixed-phase P25 was composed of individual single-crystal particles of anatase and rutile rather than anatase particles covered by a layer of rutile. Subsequently, their view was confirmed by Zhang et al. [130] and Ohno et al. [131]. But they did not further study the mechanism of the enhanced photocatalytic performance of the mixed-phase $TiO_2$.

In 2002, Kawahara et al. [132] designed a film model to confirm the migration direction of the photo-generated excitons in anatase/rutile mixed-phase crystal $TiO_2$ under light irradiation. The mixed-phase crystal $TiO_2$ film was immersed into an $AgNO_3$ solution with the exposure to light over a period of time at the atmosphere of argon. It could be observed that there were a large number of Ag particles appearing on the surface of the rutile phase. According to the phenomenon, they inferred that $Ag^+$ caused a reduction reaction on the rutile surface and the photo-generated electrons migrated from the conduction band of anatase to rutile, as shown in Fig. 6.20.

In 2003, Sun et al. [134, 135] deposited Pt on P25 and applied the catalyst to the photocatalytic degradation of phenol. They found that loading P25 with Pt did not show the increase of photocatalytic activity for phenol decomposition as well as the total carbon removal rates. Besides, they found that Pt appeared on the surface of anatase. Therefore, as shown in Fig. 6.21, they proposed a charge separation

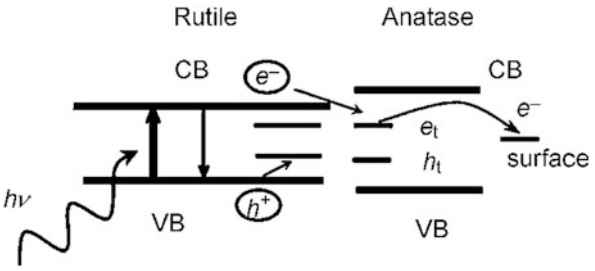


**Fig. 6.22** A proposed schematic illustration showing the separation of photo-generated holes and electrons using EPR [51]. (Reprinted with permission from Ref. [51]. Copyright 2003, American Chemical Society)

mechanism for P25 that the contact of the two phases led to the bending of the conduction band, resulting in the holes in anatase transferring to rutile, while the electrons in anatase not transferring to rutile, further causing the results that holes were concentrated in rutile and electrons stayed in the anatase particles. It was to say that the oxidation reaction mostly happened on rutile and the reduction reactions mostly took place on anatase; thus the Pt deposition on anatase was not able to increase the photocatalytic efficiency for phenol oxidation in water.

Hurum et al. [51] characterized the charge separation process of P25 via electron paramagnetic resonance (EPR) in the same year. Due to the wide bandgap of anatase, no exciton was generated under the visible light irradiation. However, the electron trapping sites were found on anatase surface in electron paramagnetic resonance spectroscopy. It could be concluded that the electrons in rutile excited by visible light transferred to the lower-energy anatase lattice trapping sites, improving the separation charges and thus enhancing the photocatalytic activity of P25 (Fig. 6.22). Thereafter, Liu et al. [136] confirmed this mechanism via the photocatalytic activity experiments of anatase/rutile mixed-phase $TiO_2$ nanotubes.

EPR spectroscopy is a new characterization method which has been developed in recent years. It can be used for the detection of the unpaired electrons in the sample. Many researchers have started to characterize the migration behaviors of photo-generated electrons and holes in the mixed-phase $TiO_2$ via the EPR technique [137].

An "antenna mechanism" was proposed to explain the mechanism of improved photocatalytic performance in mixed crystal phases by Wang et al. [138] in 2006. They thought that during the photocatalytic degradation process, $TiO_2$ absorbed light to produce photo-generated excitons, which then take part in the oxidation–reduction reactions with the target molecules adsorbed on the catalyst's surface; however, due to the lack of light in the depth, the particles deeper in the liquid could only receive the photon energy via the particles irradiated by light. The energy transferred from the shallow particles induced the oxidation–reduction reaction of the particles which light cannot reach, enhancing the photocatalytic activity. The long-chain particles served as an antenna to transfer the photon energy from the location of light absorption to the location of reaction in the process of photon energy being transferred to the photocatalyst deeper in the liquid; thus this is called an "antenna mechanism" (Fig. 6.23).

However, the theoretical models in the research objects mentioned above are all P25 consisting of a certain phase ratio of anatase and rutile. Because mixed-phase

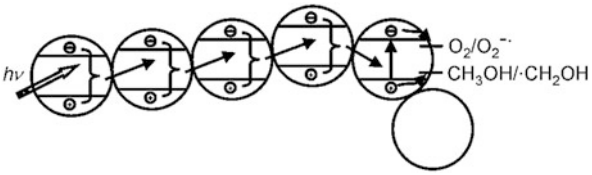


**Fig. 6.23** Antenna effect by network structure leading to the enhancement of photocatalytic activity [138]. (Reprinted with permission from Ref. [138]. Copyright, 2006 Elsevier)

$TiO_2$ with different phase ratios exhibit different photocatalytic activities, it is difficult to adequately explain the physical phenomenon responsible for the existence of an optimum phase ratio in mixed-phase $TiO_2$ with the maximum photocatalytic activity using these existing models. Therefore, further research is essential to find out the photocatalytic mechanism of mixed-phase $TiO_2$ in different phase contents.

In 2008, Zachariah et al. [103] took the factors of crystallite size distribution as well as phase composition into account, and proposed a new mechanism model, which overcame the limitations of the existing models in terms of explaining the abovementioned phenomenon. The mechanism is based on the charge separation mechanism proposed by Sun et al. [134]. Zachariah et al. [103] thought that when the size of nano-$TiO_2$ was identical (Fig. 6.24a), the bandgap of adjacent anatase crystallites was the same, so there was no driving force to migrate the photo-generated holes, resulting in the high recombination rate of photo-generated charges and the low photocatalytic activity. If the sizes of anatase crystallite were different and were below the critical size (Fig. 6.24b, c), the bandgaps of the connected crystallites would depend on their size. Thus, photo-generated holes in one crystallite could easily escape into the other, leading to the effective separation of photo-generated excitons. When a small amount of rutile was mixed with anatase (Fig. 6.24d), owing to the different bandgap, photo-generated holes would transfer from anatase to rutile, so that the photocatalytic activity could be further enhanced. However, the excessive rutile content limited the migration of photo-generated holes in mixed-phase crystal $TiO_2$ (Fig. 6.24e), and the photocatalytic activity of photocatalysts began to decline. On the condition that the crystallite sizes of pure rutile are bigger than the critical size (Fig. 6.24f), their bandgap values kept the same, and then the migration of photo-generated holes could not occur, and the photocatalytic activity was minimum. The mechanism showed that whether the $TiO_2$ was mixed-phase crystalline or single crystalline, the photo-generated electron–hole pairs could be separated and the photocatalytic activity of photocatalysts could be enhanced as long as the bandgap values were different.

In summary, the mechanisms mentioned above for the enhanced photocatalytic activity of mixed-phase $TiO_2$ all involve the migration behaviors of photo-generated excitons. In these mechanisms, researchers all agree that the mixed-phase crystal structure favors the effective separation of photo-generated electrons and holes. However, the specific migration paths of excitons are still controversial. The

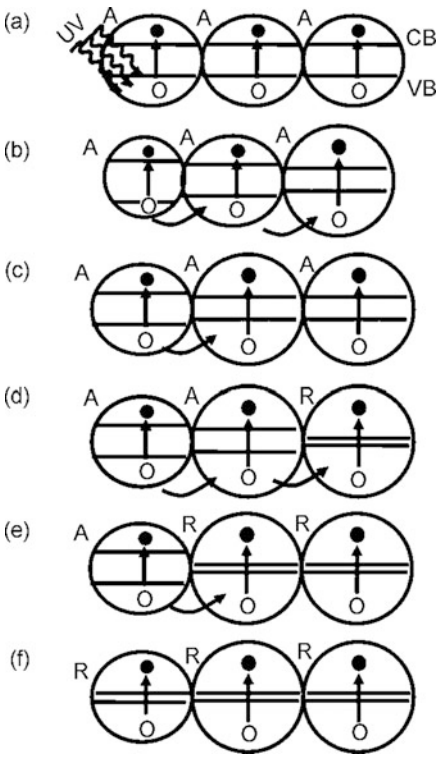


**Fig. 6.24** A schematic illustration of the newly proposed mechanism in the basis of the bandgap variation in the connected nanocrystallites as a function of the phase and the size distribution involved [103]. A, R, CB, and VB stand for anatase $TiO_2$, rutile $TiO_2$, the conduction band, and the valence band, respectively [103]. (Reprinted with permission from Ref. [103]. Copyright 2009, American Chemical Society)

determining factors for the photocatalytic activity of mixed-phase crystal $TiO_2$ contain grain size, structural forms (core–shell structure, cladding structure, random composite, etc.), phase composition, and so on. These factors cause the emergence of bending band, trapping sites, and other phenomena in the mixed-phase $TiO_2$. Therefore, the obtained mixed-phase $TiO_2$ differ in photocatalytic mechanism on different experimental conditions, so further research is still required.

## 6.6 Conclusion and Outlook

In the field of photocatalysis, since it was discovered that $TiO_2$ nanomaterials could be used for photocatalytic water splitting and degradation of organic pollutants in the 1970s, the synthetic methods and applications of mixed-phase $TiO_2$ have achieved great progress. The superior photocatalytic performance of mixed-phase $TiO_2$ to single-phase $TiO_2$ has been well recognized, and the mechanism of the improved photocatalytic activities of the mixed-phase $TiO_2$ photocatalysts has also been widely studied. However, there are still many problems remaining to be resolved. For instance, (1) particulate mixed-phase $TiO_2$ nanomaterials are easy to agglomerate, which will greatly inhibit the photocatalytic activity and impede the further

development of the materials; (2) though the relatively narrow bandgap of rutile is able to extend the absorption of the mixed-phase $TiO_2$ to some of the visible light range, it is still unable to completely utilize all visible light from sunlight, limiting its practical application in photocatalysis; and (3) although researchers all approve that the mixed-phase crystal structure favors the effective separation of photo-generated electrons and holes, thereby improving the photocatalytic activity, there is still much controversy about the mobility direction of photo-generated excitons. It is necessary for researchers to further study on the mechanism of the enhanced photocatalytic performance of mixed-phase $TiO_2$. Therefore, developing the mixed-phase $TiO_2$ nanomaterials, combining other advantageous structures (such as hierarchical structure) to enhance the utilization of the visible light, and exploring the mechanism of photocatalytic reactions by newly developed characterization techniques will retain as the challenges and hot research themes in the future.

Although mixed-phase $TiO_2$ photocatalysts have been studied for decades, it is still a hot research theme owing to its excellent photocatalytic activity. With the increase of serious energy crisis and environmental problems, the applications of mixed-phase crystal $TiO_2$ are predicted to attract lasting and considerable attention.

## References

1. Fujishima A, Honda K (1972) Electrochemical photolysis of water at a semiconductor electrode. Nature 238(5358):37–38
2. Carey JH, Lawrence J, Tosine HM (1976) Photodechlorination of PCB's in the presence of titanium dioxide in aqueous suspensions. Bull Environ Contam Toxicol 16(6):697–701
3. Habisreutinger SN, Schmidt-Mende L, Stolarczyk JK (2013) Photocatalytic reduction of $CO_2$ on $TiO_2$ and other semiconductors. Angew Chem Int Ed 52(29):7372–7408
4. Hu K, Robson KC, Johansson PG et al (2012) Intramolecular hole transfer at sensitized $TiO_2$ interfaces. J Am Chem Soc 134(20):8352–8355
5. Guo Q, Xu C, Ren Z et al (2012) Stepwise photocatalytic dissociation of methanol and water on $TiO_2$ (110). J Am Chem Soc 134(32):13366–13373
6. Tian B, Chen F, Zhang J et al (2006) Influences of acids and salts on the crystalline phase and morphology of $TiO_2$ prepared under ultrasound irradiation. J Colloid Interface Sci 303 (1):142–148
7. Tomkiewicz M, Dagan G, Zhu Z (1994) Morphology and photocatalytic activity of $TiO_2$ aerogels. Res Chem Intermed 20(7):701–710
8. Zhu S, Xie G, Yang X et al (2013) A thick hierarchical rutile $TiO_2$ nanomaterial with multilayered structure. Mater Res Bull 48(5):1961–1966
9. Beuvier T, Richard-Plouet M, Mancini-Le Granvalet M et al (2010) $TiO_2$ (B) nanoribbons as negative electrode material for lithium ion batteries with high rate performance. Inorg Chem 49(18):8457–8464
10. Xin X, Scheiner M, Ye M et al (2011) Surface-treated $TiO_2$ nanoparticles for dye-sensitized solar cells with remarkably enhanced performance. Langmuir 27(23):14594–14598
11. Hosono E, Fujihara S, Imai H et al (2007) One-step synthesis of nano–micro chestnut $TiO_2$ with rutile nanopins on the microanatase octahedron. ACS Nano 1(4):273–278
12. Sinha AK, Jana S, Pande S et al (2009) New hydrothermal process for hierarchical $TiO_2$ nanostructures. Cryst Eng Comm 11(7):1210–1212

13. Cheng QQ, Cao Y, Yang L et al (2011) Synthesis and photocatalytic activity of titania microspheres with hierarchical structures. Mater Res Bull 46(3):372–377
14. Wang Y, Zhang L, Deng K et al (2007) Low temperature synthesis and photocatalytic activity of rutile $TiO_2$ nanorod superstructures. J Phys Chem C 111(6):2709–2714
15. Wei J, Yao J, Zhang X et al (2007) Hydrothermal growth of titania nanostructures with tunable phase and shape. Mater Lett 61(23):4610–4613
16. Hu YH (2012) A highly efficient photocatalyst—hydrogenated black $TiO_2$ for the photocatalytic splitting of water. Angew Chem Int Ed 51(50):12410–12412
17. Oh JK, Lee JK, Kim HS et al (2010) $TiO_2$ branched nanostructure electrodes synthesized by seeding method for dye-sensitized solar cells. Chem Mater 22(3):1114–1118
18. Ye M, Liu HY, Lin C et al (2013) Hierarchical rutile $TiO_2$ flower cluster-based high efficiency dye-sensitized solar cells via direct hydrothermal growth on conducting substrates. Small 9 (2):312–321
19. Si P, Ding S, Yuan J et al (2011) Hierarchically structured one-dimensional $TiO_2$ for protein immobilization, direct electrochemistry, and mediator-free glucose sensing. ACS Nano 5 (9):7617–7626
20. Etgar L, Gao P, Xue Z et al (2012) Mesoscopic $CH_3 NH_3 PbI_3/TiO_2$ heterojunction solar cells. J Am Chem Soc 134(42):17396–17399
21. Guo W, Xu C, Wang X et al (2012) Rectangular bunched rutile $TiO_2$ nanorod arrays grown on carbon fiber for dye-sensitized solar cells. J Am Chem Soc 134(9):4437–4441
22. Wang YQ, Gu L, Guo YG et al (2012) Rutile-$TiO_2$ nanocoating for a high-rate $Li_4Ti_5O_{12}$ anode of a lithium-ion battery. J Am Chem Soc 134(18):7874–7879
23. So S, Lee K, Schmuki P (2012) Ultrafast growth of highly ordered anodic $TiO_2$ nanotubes in lactic acid electrolytes. J Am Chem Soc 134(28):11316–11318
24. Wang WN, An WJ, Ramalingam B et al (2012) Size and structure matter: enhanced $CO_2$ photoreduction efficiency by size-resolved ultrafine Pt nanoparticles on $TiO_2$ single crystals. J Am Chem Soc 134(27):11276–11281
25. Leghari SAK, Sajjad S, Chen F et al (2011) $WO_3/TiO_2$ composite with morphology change via hydrothermal template-free route as an efficient visible light photocatalyst. Chem Eng J 166 (3):906–915
26. Chen F, Zou W, Qu W et al (2009) Photocatalytic performance of a visible light $TiO_2$ photocatalyst prepared by a surface chemical modification process. Catal Commun 10 (11):1510–1513
27. Xing M, Zhang J, Chen F (2009) New approaches to prepare nitrogen-doped $TiO_2$ photocatalysts and study on their photocatalytic activities in visible light. Appl Catal B Environ 89(3):563–569
28. Kim TH, Gómez-Solís C, Moctezuma E et al (2014) Sonochemical synthesis of Fe–$TiO_2$–SiC composite for degradation of rhodamine B under solar simulator. Res Chem Intermed 40 (4):1595–1605
29. Zuo F, Wang L, Wu T et al (2010) Self-doped $Ti^{3+}$ enhanced photocatalyst for hydrogen production under visible light. J Am Chem Soc 132(34):11856–11857
30. Kim YJ, Lee MH, Kim HJ et al (2009) Formation of highly efficient dye-sensitized solar cells by hierarchical pore generation with nanoporous $TiO_2$ spheres. Adv Mater 21(36):3668–3673
31. Liu S, Li Q, Hou C et al (2013) Hierarchical nitrogen and cobalt co-doped $TiO_2$ prepared by an interface-controlled self-aggregation process. J Alloys Compd 575:128–136
32. Cai M, Pan X, Liu W et al (2013) Multiple adsorption of tributyl phosphate molecule at the dyed-$TiO_2$/electrolyte interface to suppress the charge recombination in dye-sensitized solar cell. J Mater Chem A 1(15):4885–4892
33. Liang MS, Khaw CC, Liu CC et al (2013) Synthesis and characterisation of thin-film $TiO_2$ dye-sensitised solar cell. Ceram Int 39(2):1519–1523
34. Kim H, Hwang YH, Cho G et al (2011) Partially dyed-$TiO_2$ dispersions for adaptation to the continuous fabrication of photoanodes. Electrochim Acta 56(25):9476–9481

35. Zhang C, Huang Y, Chen S et al (2012) Photoelectrochemical analysis of the dyed $TiO_2$/electrolyte interface in long-term stability of dye-sensitized solar cells. J Phys Chem C 116 (37):19807–19813
36. Bae EG, Kim H, Hwang YH et al (2012) Genetic algorithm-assisted optimization of partially dyed-$TiO_2$ for room-temperature printable photoanodes of dye-sensitized solar cells. J Mater Chem 22(2):551–556
37. Ashkarran AA, Ghavamipour M, Hamidinezhad H et al (2015) Enhanced visible light-induced hydrophilicity in sol–gel-derived Ag–$TiO_2$ hybrid nanolayers. Res Chem Intermed 41 (10):7299–7311
38. Haruta M, Uphade BS, Tsubota S et al (1998) Selective oxidation of propylene over gold deposited on titanium-based oxides. Res Chem Intermed 24(3):329–336
39. Tian B, Zhang J, Tong T et al (2008) Preparation of Au/$TiO_2$ catalysts from Au (I)–thiosulfate complex and study of their photocatalytic activity for the degradation of methyl orange. Appl Catal B Environ 79(4):394–401
40. Wu Y, Liu H, Zhang J et al (2009) Enhanced photocatalytic activity of nitrogen-doped titania by deposited with gold. J Phys Chem C 113(33):14689–14695
41. Wang W, Zhang J, Chen F et al (2010) Catalysis of redox reactions by Ag@$TiO_2$ and $Fe^{3+}$-doped Ag@$TiO_2$ core–shell type nanoparticles. Res Chem Intermed 36(2):163–172
42. Wang Y, Feng C, Zhang M et al (2010) Enhanced visible light photocatalytic activity of N-doped $TiO_2$ in relation to single-electron-trapped oxygen vacancy and doped-nitrogen. Appl Catal B Environ 100(1):84–90
43. Feng C, Wang Y, Zhang J et al (2012) The effect of infrared light on visible light photocatalytic activity: an intensive contrast between Pt-doped $TiO_2$ and N-doped $TiO_2$. Appl Catal B Environ 113:61–71
44. Charanpahari A, Umare SS, Gokhale SP et al (2012) Enhanced photocatalytic activity of multi-doped $TiO_2$ for the degradation of methyl orange. Appl Catal A Gen 443:96–102
45. Tian B, Li C, Gu F et al (2009) Synergetic effects of nitrogen doping and Au loading on enhancing the visible-light photocatalytic activity of nano-$TiO_2$. Catal Commun 10 (6):925–929
46. Zhang P, Shao C, Li X et al (2012) In situ assembly of well-dispersed Au nanoparticles on $TiO_2$/ZnO nanofibers: a three-way synergistic heterostructure with enhanced photocatalytic activity. J Hazard Mater 237:331–338
47. Zhang Z, Yuan Y, Liang L et al (2008) Preparation and photoelectrocatalytic activity of ZnO nanorods embedded in highly ordered $TiO_2$ nanotube arrays electrode for azo dye degradation. J Hazard Mater 158(2):517–522
48. Chattopadhyaya G, Macdonald DG, Bakhshi NN et al (2006) Removal of nitric oxide over Saskatchewan lignite and its derivatives. Catal Lett 108(1):1–5
49. Yang M, Men Y, Li S et al (2012) Enhancement of catalytic activity over $TiO_2$-modified $Al_2O_3$ and ZnO–$Cr_2O_3$ composite catalyst for hydrogen production via dimethyl ether steam reforming. Appl Catal A Gen 433:26–34
50. Su R, Bechstein R, Sø L et al (2011) How the anatase-to-rutile ratio influences the photoreactivity of $TiO_2$. J Phys Chem C 115(49):24287–24292
51. Hurum DC, Agrios AG, Gray KA et al (2003) Explaining the enhanced photocatalytic activity of Degussa P25 mixed-phase $TiO_2$ using EPR. J Phys Chem B 107(19):4545–4549
52. Scotti R, Bellobono IR, Canevali C et al (2008) Sol−gel pure and mixed-phase titanium dioxide for photocatalytic purposes: relations between phase composition, catalytic activity, and charge-trapped sites. Chem Mater 20(12):4051–4061
53. Puddu V, Choi H, Dionysiou DD et al (2010) $TiO_2$ photocatalyst for indoor air remediation: influence of crystallinity, crystal phase, and UV radiation intensity on trichloroethylene degradation. Appl Catal B Environ 94(3):211–218
54. Zheng R, Meng X, Tang F (2009) Synthesis, characterization and photodegradation study of mixed-phase titania hollow submicrospheres with rough surface. Appl Surf Sci 255 (11):5989–5994

55. Jiao Y, Chen F, Zhao B et al (2012) Anatase grain loaded brookite nanoflower hybrid with superior photocatalytic activity for organic degradation. Colloids Surf A Physicochem Eng Asp 402:66–71
56. Di Paola A, Cufalo G, Addamo M et al (2008) Photocatalytic activity of nanocrystalline $TiO_2$ (brookite, rutile and brookite-based) powders prepared by thermohydrolysis of $TiCl_4$ in aqueous chloride solutions. Colloids Surf A Physicochem Eng Asp 317(1):366–376
57. Li W, Liu C, Zhou Y et al (2008) Enhanced photocatalytic activity in anatase/$TiO_2$ (B) core−shell nanofiber. J Phys Chem C 112(51):20539–20545
58. Hanaor DA, Sorrell CC (2011) Review of the anatase to rutile phase transformation. J Mater Sci 46(4):855–874
59. Gamboa JA, Pasquevich DM (1992) Effect of chlorine atmosphere on the anatase-rutile transformation. J Am Ceram Soc 75(11):2934–2938
60. Ding XZ, He YZ (1996) Study of the room temperature ageing effect on structural evolution of gel-derived nanocrystalline titania powders. J Mater Sci Lett 15(4):320–322
61. Muscat J, Swamy V, Harrison NM (2002) First-principles calculations of the phase stability of $TiO_2$. Phys Rev B 65(22):224–112
62. Arlt T, Bermejo M, Blanco MA et al (2000) High-pressure polymorphs of anatase $TiO_2$. Phys Rev B 61(21):14414–14419
63. Ren R, Yang Z, Shaw LL (2000) Polymorphic transformation and powder characteristics of $TiO_2$ during high energy milling. J Mater Sci 35(23):6015–6026
64. Dubrovinskaia NA, Dubrovinsky LS, Ahuja R et al (2001) Experimental and theoretical identification of a new high-pressure $TiO_2$ polymorph. Phys Rev Lett 87(27):455–475
65. Diebold U (2003) The surface science of titanium dioxide. Surf Sci Rep 48(5):53–229
66. Yan M, Chen F, Zhang J et al (2005) Preparation of controllable crystalline titania and study on the photocatalytic properties. J Phys Chem B 109(18):8673–8678
67. Li Y, White TJ, Lim SH (2004) Low-temperature synthesis and microstructural control of titania nano-particles. J Solid State Chem 177(4):1372–1381
68. Khataee AR, Kasiri MB (2010) Photocatalytic degradation of organic dyes in the presence of nanostructured titanium dioxide: influence of the chemical structure of dyes. J Mol Catal A Chem 328(1):8–26
69. Daneshvar N, Rasoulifard MH, Khataee AR et al (2007) Removal of CI acid orange 7 from aqueous solution by UV irradiation in the presence of ZnO nanopowder. J Hazard Mater 143 (1):95–101
70. Moret MP, Zallen R, Vijay DP et al (2000) Brookite-rich titania films made by pulsed laser deposition. Thin Solid Films 366(1):8–10
71. Shannon RD, Pask JA (1965) Kinetics of the anatase-rutile transformation. J Am Ceram Soc 48(8):391–398
72. Batzill M, Morales EH, Diebold U (2006) Influence of nitrogen doping on the defect formation and surface properties of $TiO_2$ rutile and anatase. Phys Rev Lett 96(2):026–103
73. Oskam G, Nellore A, Penn RL et al (2003) The growth kinetics of $TiO_2$ nanoparticles from titanium (IV) alkoxide at high water/titanium ratio. J Phys Chem B 107(8):1734–1738
74. Banfield J (1998) Thermodynamic analysis of phase stability of nanocrystalline titania. J Mater Chem 8(9):2073–2076
75. Li JG, Ishigaki T, Sun X (2007) Anatase, brookite, and rutile nanocrystals via redox reactions under mild hydrothermal conditions: phase-selective synthesis and physicochemical properties. J Phys Chem C 111(13):4969–4976
76. Bickley RI, Gonzalez-Carreno T, Lees JS et al (1991) A structural investigation of titanium dioxide photocatalysts. J Solid State Chem 92(1):178–190
77. Lee SK, Robertson PK, Mills A et al (1999) Modification and enhanced photocatalytic activity of $TiO_2$ following exposure to non-linear irradiation sources. J Photochem Photobiol A Chem 122(1):69–71
78. Tsai SJ, Cheng S (1997) Effect of $TiO_2$ crystalline structure in photocatalytic degradation of phenolic contaminants. Catal Today 33(1–3):227–237

79. Ohno T, Sarukawa K, Matsumura M (2001) Photocatalytic activities of pure rutile particles isolated from $TiO_2$ powder by dissolving the anatase component in HF solution. J Phys Chem B 105(12):2417–2420
80. Ozawa T, Iwasaki M, Tada H et al (2005) Low-temperature synthesis of anatase–brookite composite nanocrystals: the junction effect on photocatalytic activity. J Colloid Interface Sci 281(2):510–513
81. Xu H, Zhang L (2009) Controllable one-pot synthesis and enhanced photocatalytic activity of mixed-phase $TiO_2$ nanocrystals with tunable brookite/rutile ratios. J Phys Chem C 113 (5):1785–1790
82. Bacsa RR, Kiwi J (1998) Effect of rutile phase on the photocatalytic properties of nanocrystalline titania during the degradation of p-coumaric acid. Appl Catal B Environ 16(1):19–29
83. Jung KY, Park SB, Jang HD (2004) Phase control and photocatalytic properties of nano-sized titania particles by gas-phase pyrolysis of $TiCl_4$. Catal Commun 5(9):491–497
84. Zhu J, Zheng W, He B et al (2004) Characterization of Fe–$TiO_2$ photocatalysts synthesized by hydrothermal method and their photocatalytic reactivity for photodegradation of XRG dye diluted in water. J Mol Catal A Chem 216(1):35–43
85. Wu Y, Xing M, Zhang J (2011) Gel-hydrothermal synthesis of carbon and boron co-doped $TiO_2$ and evaluating its photocatalytic activity. J Hazard Mater 192(1):368–373
86. Ng J, Wang X, Sun DD (2011) One-pot hydrothermal synthesis of a hierarchical nanofungus-like anatase $TiO_2$ thin film for photocatalytic oxidation of bisphenol A. Appl Catal B Environ 110:260–272
87. Ovenstone J, Yanagisawa K (1999) Effect of hydrothermal treatment of amorphous titania on the phase change from anatase to rutile during calcination. Chem Mater 11(10):2770–2774
88. Li G, Ciston S, Saponjic ZV et al (2008) Synthesizing mixed-phase $TiO_2$ nanocomposites using a hydrothermal method for photo-oxidation and photoreduction applications. J Catal 253 (1):105–110
89. Fehse M, Fischer F, Tessier C et al (2013) Tailoring of phase composition and morphology of $TiO_2$-based electrode materials for lithium-ion batteries. J Power Sources 231:23–28
90. Zhang Y, Chen J, Li X (2010) Preparation and photocatalytic performance of anatase/rutile mixed-phase $TiO_2$ nanotubes. Catal Lett 139(3–4):129–133
91. Tay Q, Liu X, Tang Y et al (2013) Enhanced photocatalytic hydrogen production with synergistic two-phase anatase/brookite $TiO_2$ nanostructures. J Phys Chem C 117 (29):14973–14982
92. Zhang H, Banfield JF (2000) Understanding polymorphic phase transformation behavior during growth of nanocrystalline aggregates: insights from $TiO_2$. J Phys Chem B 104 (15):3481–3487
93. Shen X, Tian B, Zhang J (2013) Tailored preparation of titania with controllable phases of anatase and brookite by an alkalescent hydrothermal route. Catal Today 201:151–158
94. Zhao B, Chen F, Huang Q et al (2009) Brookite $TiO_2$ nanoflowers. Chem Commun 34:5115–5117
95. Zhao LM, Zhang ZJ, Zhang SY et al (2011) Metal–organic frameworks based on transition-metal carboxylate clusters as secondary building units: synthesis, structures and properties. CrystEngComm 13(3):907–913
96. Zhao B, Chen F, Jiao Y et al (2010) Phase transition and morphological evolution of titania/titanate nanomaterials under alkalescent hydrothermal treatment. J Mater Chem 20 (37):7990–7997
97. Shen X, Zhang J, Tian B (2012) Tartaric acid-assisted preparation and photocatalytic performance of titania nanoparticles with controllable phases of anatase and brookite. J Mater Sci 47 (15):5743–5751
98. Cheng H, Ma J, Zhao Z et al (1995) Hydrothermal preparation of uniform nanosize rutile and anatase particles. Chem Mater 7(4):663–671
99. Li G, Gray KA (2007) Preparation of mixed-phase titanium dioxide nanocomposites via solvothermal processing. Chem Mater 19(5):1143–1146

100. Lei SHI, Duan WENG (2008) Highly active mixed-phase $TiO_2$ photocatalysts fabricated at low temperature and the correlation between phase composition and photocatalytic activity. J Environ Sci 20(10):1263–1267
101. Wu M, Long J, Huang A et al (1999) Microemulsion-mediated hydrothermal synthesis and characterization of nanosize rutile and anatase particles. Langmuir 15(26):8822–8825
102. Shen X, Zhang J, Tian B (2011) Microemulsion-mediated solvothermal synthesis and photocatalytic properties of crystalline titania with controllable phases of anatase and rutile. J Hazard Mater 192(2):651–657
103. Zachariah A, Priya R, Baiju KV, Shukla S et al (2008) Synergistic effect in photocatalysis as observed for mixed-phase nanocrystalline titania processed via sol-gel solvent mixing and calcination. J Phys Chem C 112:11345–11356
104. Bojinova A, Kralchevska R, Poulios I et al (2007) Anatase/rutile $TiO_2$ composites: influence of the mixing ratio on the photocatalytic degradation of malachite green and orange II in slurry. Mater Chem Phys 106(2):187–192
105. Liu Z, Zhang X, Nishimoto S et al (2007) Anatase $TiO_2$ nanoparticles on rutile $TiO_2$ nanorods: a heterogeneous nanostructure via layer-by-layer assembly. Langmuir 23(22):10916–10919
106. Nair RG, Paul S, Samdarshi SK (2011) High UV/visible light activity of mixed phase titania: a generic mechanism. Sol Energy Mater Sol Cells 95(7):1901–1907
107. Gouma PI, Mills MJ (2001) Anatase-to-rutile transformation in titania powders. J Am Ceram Soc 84(3):619–622
108. Zhang J, Li M, Feng Z et al (2006) UV Raman spectroscopic study on $TiO_2$ I. Phase transformation at the surface and in the bulk. J Phys Chem B 110(2):927–935
109. Hsu YC, Lin HC, Chen CH et al (2010) Nonaqueous seeded growth of flower-like mixed-phase titania nanostructures for photocatalytic applications. J Solid State Chem 183 (9):1917–1924
110. Ni M, Leung MK, Leung DY et al (2007) A review and recent developments in photocatalytic water-splitting using $TiO_2$ for hydrogen production. Renew Sust Energ Rev 11(3):401–425
111. Lei J, Li H, Zhang J et al (2016) Mixed-phase $TiO_2$ nanomaterials as efficient photocatalysts. In: Low-dimensional and nanostructured materials and devices. Springer International Publishing, Cham, pp 423–460
112. Xu Q, Ma Y, Zhang J et al (2011) Enhancing hydrogen production activity and suppressing CO formation from photocatalytic biomass reforming on $Pt/TiO_2$ by optimizing anatase–rutile phase structure. J Catal 278(2):329–335
113. Kho YK, Iwase A, Teoh WY et al (2010) Photocatalytic $H_2$ evolution over $TiO_2$ nanoparticles. The synergistic effect of anatase and rutile. J Phys Chem C 114(6):2821–2829
114. Xu F, Xiao W, Cheng B et al (2014) Direct Z-scheme anatase/rutile bi-phase nanocomposite $TiO_2$ nanofiber photocatalyst with enhanced photocatalytic $H_2$-production activity. Int J Hydrog Energy 39(28):15394–15402
115. Rosseler O, Shankar MV, Karkmaz-Le Du M et al (2010) Solar light photocatalytic hydrogen production from water over Pt and $Au/TiO_2$ (anatase/rutile) photocatalysts: influence of noble metal and porogen promotion. J Catal 269(1):179–190
116. Marcı G, Addamo M, Augugliaro V et al (2003) Photocatalytic oxidation of toluene on irradiated $TiO_2$: comparison of degradation performance in humidified air, in water and in water containing a zwitterionic surfactant. J Photochem Photobiol A Chem 160(1):105–114
117. Liu L, Zhao H, Andino JM et al (2012) Photocatalytic $CO_2$ reduction with $H_2O$ on $TiO_2$ nanocrystals: comparison of anatase, rutile, and brookite polymorphs and exploration of surface chemistry. ACS Catal 2(8):1817–1828
118. Zhao H, Liu L, Andino JM et al (2013) Bicrystalline $TiO_2$ with controllable anatase–brookite phase content for enhanced $CO_2$ photoreduction to fuels. J Mater Chem A 1(28):8209–8216
119. Frank NS, Bard AJ (1977) Heterogeneous photocatalytic oxidation of cyanide ion in aqueous solutions at titanium dioxide powder. J Am Chem Soc 99(1):303–304
120. Xu H, Li G, Zhu G et al (2015) Enhanced photocatalytic degradation of rutile/anatase $TiO_2$ heterojunction nanoflowers. Catal Commun 62:52–56

121. Luo Z, Poyraz AS, Kuo CH et al (2015) Crystalline mixed phase (anatase/rutile) mesoporous titanium dioxides for visible light photocatalytic activity. Chem Mater 27(1):6–17
122. Zhao B, Chen F, Jiao Y et al (2011) Ag 0-loaded brookite/anatase composite with enhanced photocatalytic performance towards the degradation of methyl orange. J Mol Catal A Chem 348(1):114–119
123. Liao Y, Que W, Jia Q et al (2012) Controllable synthesis of brookite/anatase/rutile $TiO_2$ nanocomposites and single-crystalline rutile nanorods array. J Mater Chem 22(16):7937–7944
124. Grabowska E, Reszczyńska J, Zaleska A (2012) Mechanism of phenol photodegradation in the presence of pure and modified-$TiO_2$: a review. Water Res 46(17):5453–5471
125. Ding Z, Lu GQ, Greenfield PF (2000) Role of the crystallite phase of $TiO_2$ in heterogeneous photocatalysis for phenol oxidation in water. J Phys Chem B 104(19):4815–4820
126. Tian B, Li C, Zhang J (2012) One-step preparation, characterization and visible-light photocatalytic activity of Cr-doped $TiO_2$ with anatase and rutile bicrystalline phases. Chem Eng J 191:402–409
127. Deák P, Aradi B, Frauenheim T (2011) Band lineup and charge carrier separation in mixed rutile-anatase systems. J Phys Chem C 115(8):3443–3446
128. Scanlon DO, Dunnill CW, Buckeridge J et al (2013) Band alignment of rutile and anatase $TiO_2$. Nat Mater 12(9):798–801
129. Datye AK, Riegel G, Bolton JR et al (1995) Microstructural characterization of a fumed titanium dioxide photocatalyst. J Solid State Chem 115(1):236–239
130. Zhang Z, Wang CC, Zakaria R et al (1998) Role of particle size in nanocrystalline $TiO_2$-based photocatalysts. J Phys Chem B 102(52):10871–10878
131. Ohno T, Sarukawa K, Tokieda K et al (2001) Morphology of a $TiO_2$ photocatalyst (Degussa, P-25) consisting of anatase and rutile crystalline phases. J Catal 203(1):82–86
132. Kawahara T, Konishi Y, Tada H et al (2002) A patterned $TiO_2$ (anatase)/$TiO_2$ (rutile) bilayer-type photocatalyst: effect of the anatase/rutile junction on the photocatalytic activity. Angew Chem 114(15):2935–2937
133. Li G, Gray KA (2007) The solid–solid interface: explaining the high and unique photocatalytic reactivity of $TiO_2$-based nanocomposite materials. Chem Phys 339(1):173–187
134. Sun B, Vorontsov AV, Smirniotis PG (2003) Role of platinum deposited on $TiO_2$ in phenol photocatalytic oxidation. Langmuir 19(8):3151–3156
135. Sun B, Smirniotis PG (2003) Interaction of anatase and rutile $TiO_2$ particles in aqueous photooxidation. Catal Today 88(1):49–59
136. Liu B, Peng L (2013) Facile formation of mixed phase porous $TiO_2$ nanotubes and enhanced visible-light photocatalytic activity. J Alloys Compd 571:145–152
137. Li G, Chen L, Graham ME et al (2007) A comparison of mixed phase titania photocatalysts prepared by physical and chemical methods: the importance of the solid–solid interface. J Mol Catal A Chem 275(1):30–35
138. Wang CY, Pagel R, Dohrmann JK et al (2006) Antenna mechanism and deaggregation concept: novel mechanistic principles for photocatalysis. C R Chim 9(5):761–773